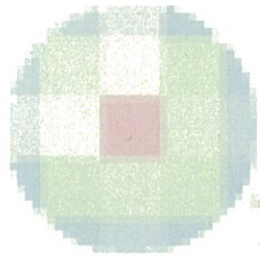


16. Pan HC, Sheehan J, Stroila M, Steiner M, Steiner L. Late cyst formation following gamma knife surgery of arteriovenous malformations. *J Neurosurg* 2005;102 Suppl: 124-7.
17. Safavi-Abbasi S, Feiz-Erfan I, Spetzler RF, Kim L, Dogan S, Porter RW, et al. Hemorrhage of cavernous malformations during pregnancy and in the peripartum period: Causal or coincidence? Case report and review of the literature. *Neurosurg Focus* 2006;21:e12.
18. Schultheiss TE, Kun LE, Ang KK, Stephens LC. Radiation response of the central nervous system. *Int J Radiat Oncol Biol Phys* 1995;31:1093-112.
19. Shuto T, Ohtake M, Matsunaga S. Proposed mechanism for cyst formation and enlargement following Gamma Knife Surgery for arteriovenous malformations. *J Neurosurg* 2012;117 Suppl: 135-43.
20. Tewari KS, Cappuccini F, Asrat T, Flamm BL, Carpenter SE, Disaia PJ, et al. Obstetric emergencies precipitated by malignant brain tumors. *Am J Obstet Gynecol* 2000;182:1215-21.
21. Watanabe T, Saito N, Hirato J, Shimaguchi H, Fujimaki H, Sasaki T. Facial neuropathy due to axonal degeneration and microvasculitis following gamma knife surgery for vestibular schwannoma: A histological analysis. Case report. *J Neurosurg* 2003;99:916-20.
22. Weyand RD, MacCarty CS, Wilson RB. The effect of pregnancy on intracranial meningiomas occurring about the optic chiasm. *Surg Clin North Am* 1951;31:1225-33.
23. Yen CP, Jain S, Haq IU, Jagannathan J, Schlesinger D, Sheehan J, et al. Repeat gamma knife surgery for incompletely obliterated cerebral arteriovenous malformations. *Neurosurgery* 2010;67(1):55-64.





Identification of a novel cell-penetrating peptide targeting human glioblastoma cell lines as a cancer-homing transporter



Moritoshi Higa^a, Chiaki Katagiri^b, Chigusa Shimizu-Okabe^c, Tomoyuki Tsumuraya^a, Masanori Sunagawa^a, Mariko Nakamura^a, Shogo Ishiuchi^b, Chitoshi Takayama^c, Eisaku Kondo^d, Masayuki Matsushita^{a,*}

^a Department of Molecular and Cellular Physiology, Graduate School of Medicine, University of the Ryukyus, 903-0215 Okinawa, Japan

^b Department of Neurosurgery, Graduate School of Medicine, University of the Ryukyus, 903-0215 Okinawa, Japan

^c Department of Molecular Anatomy, Graduate School of Medicine, University of the Ryukyus, 903-0215 Okinawa, Japan

^d Division of Molecular and Cellular Pathology, Niigata University Graduate School of Medical and Dental Sciences, 1-757 Asahimachi-dori, Chuou-ku, Niigata 951-8510, Japan

ARTICLE INFO

Article history:

Received 15 December 2014

Available online 3 January 2015

Keywords:

CPP
DDS
Peptide
Glioblastoma
Cancer

ABSTRACT

Cell-penetrating peptides (CPPs) as a novel biomedical delivery system have been highly anticipated, since they can translocate across biological membranes and are capable of transporting their cargo inside live cells with minimal invasiveness. However, non-selective internalization in various cell types remains a challenge in the clinical application of CPPs, especially in cancer treatment. In this study, we attempted to identify novel cancer-homing CPPs to target glioblastoma multiforme (GBM), which is often refractory and resistant to treatment. We screened for CPPs showing affinity for the human GBM cell line, U87MG, from an mRNA display random peptide library. One of the candidate peptides which amino-acid sequence was obtained from the screening showed selective cell-penetrating activity in U87MG cells. Conjugation of the p16^{INK4a} functional peptide to the GBM-selective CPP induced cellular apoptosis and reduced phosphorylated retinoblastoma protein levels. This indicates that the CPP was capable of delivering a therapeutic molecule into U87MG cells inducing apoptosis. These results suggest that the novel CPP identified in this study permeates with high affinity into GBM cells, revealing it to be a promising imaging and therapeutic tool in the treatment of glioblastoma.

© 2014 Elsevier Inc. All rights reserved.

1. Introduction

Glioblastoma multiforme (GBM, WHO grade IV astrocytoma) is the most common malignant brain tumor originating in the central nervous system in adults. Despite advances in surgical resection, chemotherapy, and radiotherapy combined with adjuvant therapy, the median survival in patients with GBM is generally less than 12 months after the time of diagnosis because of its rapid progression and invasive nature [1]. Thus, there is an urgent need for more effective therapeutic strategies for refractory GBM.

Recently, cell-penetrating peptides (CPPs), also referred to as protein transduction domains (PTDs), which have the ability to permeate across the plasma membrane and can facilitate the efficient cellular internalization of biomolecules, have attracted attention as peptide-based delivery systems [2,3]. To date, CPPs such as the human immunodeficiency virus type1 (HIV-1) transcriptional activator TAT protein [4], the Antennapedia (Antp) homeodomain

of *Drosophila* [5], and poly-arginine ((Arg)_n, n = 4–16) [6,7] have been the most widely studied with respect to enhancing the intracellular delivery of CPP-conjugated molecules. Since these peptides could efficiently deliver a variety of biological macromolecules, including proteins, peptides, DNAs, RNAs and nanoparticles into various living cells with minimal cytotoxicity, the use of CPPs as a delivery system to directly introduce biologically active molecules into cells has been expected [2,8,9]. However, from a clinical point of view, non-selective internalization of CPPs into various cells is the limiting factor for cell-type or tissue specific targeting applications such as cancer treatments [4,10]. Development of target-selective CPPs may contribute to improving therapeutic efficacy and reducing side effects on normal tissues [11,12]. Accordingly, the purpose of the present study was to identify novel CPPs targeting GBM as selective transporters.

mRNA displayed peptides comprise a genotype (mRNA/cDNA) template and phenotype (nascent protein) that is encoded by its mRNA, and are linked by a covalent bond through the puromycin linker [13]. The *in vitro* cell-free protein synthesis system boasts a diversity of approximately 10¹²–10¹³ individual sequences, each

* Corresponding author. Fax: +81 98 895 1402.

E-mail address: masayuki@med.u-ryukyuu.ac.jp (M. Matsushita).

containing 10 contiguous random amino acids that are encoded by a synthetic cDNA library (templates), which is greater than that of phage display technology ($<10^9$) [14]. The amino acid sequence of an mRNA displayed polypeptide can be identified easily by nucleic acid sequencing [15,16]. Thus, mRNA display technology provides a means of screening for useful physiologically active peptides and novel functional proteins. Here, we aimed to investigate novel CPPs with an affinity for the U87MG human GBM cell line using an mRNA display random peptide library *in vitro*. In this article, we present a novel CPP as a potential tool for GBM selective intracellular delivery.

2. Materials & methods

2.1. Peptide synthesis

All peptides in the present study were synthesized chemically by SIGMA-ALDRICH (Tokyo, Japan). Peptide purity was 90% or greater, which was confirmed by high-performance liquid chromatography analysis and mass spectroscopy. Peptides were dissolved in distilled water to generate 1 mM stock solutions.

2.2. Cell culture

The human glioblastoma (GBM) cell line U87MG used in the present study was purchased from the American Type Culture Collection (USA). The other cell lines used for *in vitro* assays are shown in Table 1. All human cell lines were maintained in Dulbecco's modified Eagle's medium (DMEM) (Invitrogen) supplemented with 10% (v/v) heat-inactivated fetal bovine serum (FBS) (Invitrogen), 100 U/ml penicillin, and 100 μ g/ml streptomycin (Invitrogen) at 37 °C with 5% CO₂. Primary cultured neurons were obtained from the hippocampus of 18-embryonic-day fetal C57BL/6J mice and maintained in neurobasal medium supplemented with 2% B-27 (Invitrogen), 1% penicillin/streptomycin, and 0.5 mM L-glutamine.

2.3. Fluorescence cellular imaging and quantitative analysis

Cells were seeded at a density of 3×10^5 cells per 35 mm glass bottom dish and incubated with 10 μ M of FITC-labeled peptides in complete medium for 2 h at 37 °C. For fluorescence microscopy imaging, cells were washed twice with fresh medium, and cell fluorescence was immediately analyzed using confocal laser scanning microscopy (CLSM) (Olympus Tokyo Japan, FLUOVIEW FV-1000) without fixation. Fluorescence intensities at the region of interest (ROI) of 3 cells per microscopic image were measured by MetaMorph software Version 6 (Olympus), and experiments were conducted in triplicate. Background fluorescence intensity was subtracted from all experiments. For fluorescence-activated cells

sorting (FACS) analysis, the cells were washed twice with phosphate-buffered saline (PBS) and collected by trypsinization. Detached cells were resuspended in FACS buffer (PBS, 2% FBS), then samples (1×10^4 cells) were immediately subjected to flow cytometric analysis (MILLIPORE Guava Easy Cyte Plus) using guava soft version2 (MILLIPORE) without fixation.

2.4. RT-PCR

Total RNA was extracted with TRIzol (Invitrogen) from the human glioblastoma cell lines U87MG and U118MG, and HeLa cells. cDNA was synthesized from the RNA product using an oligo (dT) primer and cDNA synthesis kit (TAKARA) according to the manufacturer's instructions. Reverse transcription-PCR was performed with Ex-Taq polymerase (TAKARA) under the following amplification conditions: denaturation at 94 °C for 2 min, followed by 40 cycles of denaturation at 98 °C for 10 s, annealing at 55 °C for 30 s, extension at 72 °C for 2 min, and a final extension at 72 °C for 10 min. The sense/antisense primer sequences for human p16^{INK4a} were 5'-TTCCTGGACACGCTGGTGGTG-3' and 5'-GGCATCTATGCGGG CATGGTTA-3', respectively. Actin was used as internal standard gene.

2.5. Detection of apoptotic cells

U87MG cells were seeded at a density of 5×10^5 cells per 60 mm dish and incubated with 20 μ M of peptide1NSA-p16 MIS or peptide1NSA-p16 V95E in complete medium for 4 h at 37 °C, respectively. After treatment, the cells were washed twice with PBS and collected by trypsinization. Then, the cells were resuspended in 100 μ l of binding buffer (0.5 M HEPES pH 7.4, 1 M NaCl, 1 M KCl, 1 M MgCl₂, 0.2 M CaCl₂) containing 5 μ l FITC-Annexin V (BD Pharmingen) and 5 μ l Propidium iodide (PI) (SIGMA-ALDRICH), and incubated under darkness for 15 min according to the manufacturer's instructions. The cells were immediately subjected to flow cytometric analysis at 1×10^4 cells per sample.

2.6. Western blotting

U87MG cells were seeded at a density of 3×10^5 cells to 35 mm well plate and incubated with 20 μ M of peptide1NSA-p16 MIS or peptide1NSA-p16 V95E in DMEM under a serum free condition for 24 h at 37 °C, respectively. After treatment, the cells were washed with complete medium and further incubated at 37 °C for 4 h. Then, the cells were lysed with 2 \times SDS sample buffer, and extracts were separated by sodium dodecyl sulfate polyacrylamide gel electrophoresis (SDS-PAGE) using an 8% SDS-PAGE gel and transferred onto a nitrocellulose membrane (BIO-RAD). After blocking with Blocking One (NACALAI TESQUE), the membrane was sequentially probed with the following antibodies: primary antibodies were rabbit polyclonal anti-Ser 807/811 phosphorylated pRB antibody 1:1000 (CST, Cell Signaling Technology), and anti-actin monoclonal antibody 1:3000 (Chemicon); secondary antibodies were anti-rabbit antibody 1:3000 (CST), and anti-mouse antibody 1:3000 (Millipore). After washing with Tris-buffered saline Tween solution (TBS-T), signals were detected using ECL Prime Western Blotting Detection Reagent (GE Healthcare) and Versa Doc (BIO-RAD). Quantifications were carried out by densitometric analysis using Quantity One software (BIO-RAD).

2.7. Statistical analysis

Statistical significance was calculated using Statcel 3 software (OMS publishing Inc.). A student's *t*-test was used for data analysis and *p* value <0.05 was considered statistically significant. All values

Table 1

Cell lines of histologically different origins, including human GBM, were used in the cell-penetration assay. Primary cultured mouse neurons were used as a non-neoplastic counterpart.

| Cell line | Origin (histological type) |
|-----------|----------------------------------|
| U87MG | Brain (glioblastoma) |
| U118MG | Brain (glioblastoma) |
| HeLa | Uterus (squamous cell carcinoma) |
| MSTO-211H | Lung (adenocarcinoma) |
| NCI-H226 | Lung (adenocarcinoma) |
| A549 | Lung (adenocarcinoma) |
| PANC-1 | Pancreas (epithelioid carcinoma) |
| HepG2 | Liver (hepatoblastoma) |
| Caco-2 | Colon (adenocarcinoma) |
| HEK293 | Non-neoplastic, embryonic kidney |
| Neuron | Brain (mouse hippocampal neuron) |

are shown as means \pm standard deviation (SD) from at least 3 independent experiments.

3. Results

3.1. Screening for candidate CPPs targeting U87MG GBM cells

First, to identify peptides capable of permeating into glioblastoma multiforme (GBM), we screened for cell-penetrating peptides (CPPs) targeting the human GBM cell line U87MG from an mRNA display random peptide library (Fig. 1A). The mRNA display library was constructed as previously described [13]. From about 60 sequences derived from concentration libraries, we randomly selected ten candidates and synthesized chemically fluorescein isothiocyanate (FITC)-labeled peptides (Fig. 1B). Nona-arginine (RRRRRRRRR: R9) was used as a nonselective permeation CPP. To evaluate the cell-penetrating activity of these peptides, U87MG cells were incubated with 10 μ M of each numbered FITC-labeled peptide. We examined intracellular fluorescence signals in cells using confocal laser scanning microscopy (CLSM) (Fig. 1C). Moreover, we confirmed their mean fluorescence intensity using Meta Morph software (Fig. 1D). Consequently, we identified a novel CPP, peptide1 (NTCTWLKYHS), whose cell-penetrating activity was stronger than the other candidates.

3.2. Peptide1 is incorporated selectively into GBM cells

Because peptide1 showed the best cell-penetrating activity into U87MG cells, we further investigated its GBM cell selectivity using cells derived from various tissues (Table 1). Fluorescent images and quantitative analysis showed high selective permeability of the peptide1 into U87MG cells compared with other cell lines (Fig. 2A and B). As shown in Fig. 2C, FITC-labeled peptide1 also permeated into the U118MG GBM cell line. These results indicate that peptide1 might have selective permeability into GBM cells.

3.3. Peptide1-NSA exhibits increased cell-penetrating activity in U87MG cells

To improve penetration efficiency, we modified the amino acid sequence of peptide1. In one sequence, Cys (C) was substituted with Gly (G), because Cys might allow disulfide bonding to other proteins; in the other sequences, N- and/or C-terminus amino acid residues were deleted in each mutant peptide (Table 2). We synthesized seven FITC-labeled peptide1 variants, and examined intracellular fluorescence signals in U87MG cells using CLSM and flow cytometry. Images showed that the fluorescence signals of peptide1-NSA (TCTWLKYH) and peptide1-NTSA (CTWLKYH) increased compared with peptide1, although they were inferior to R9 as a

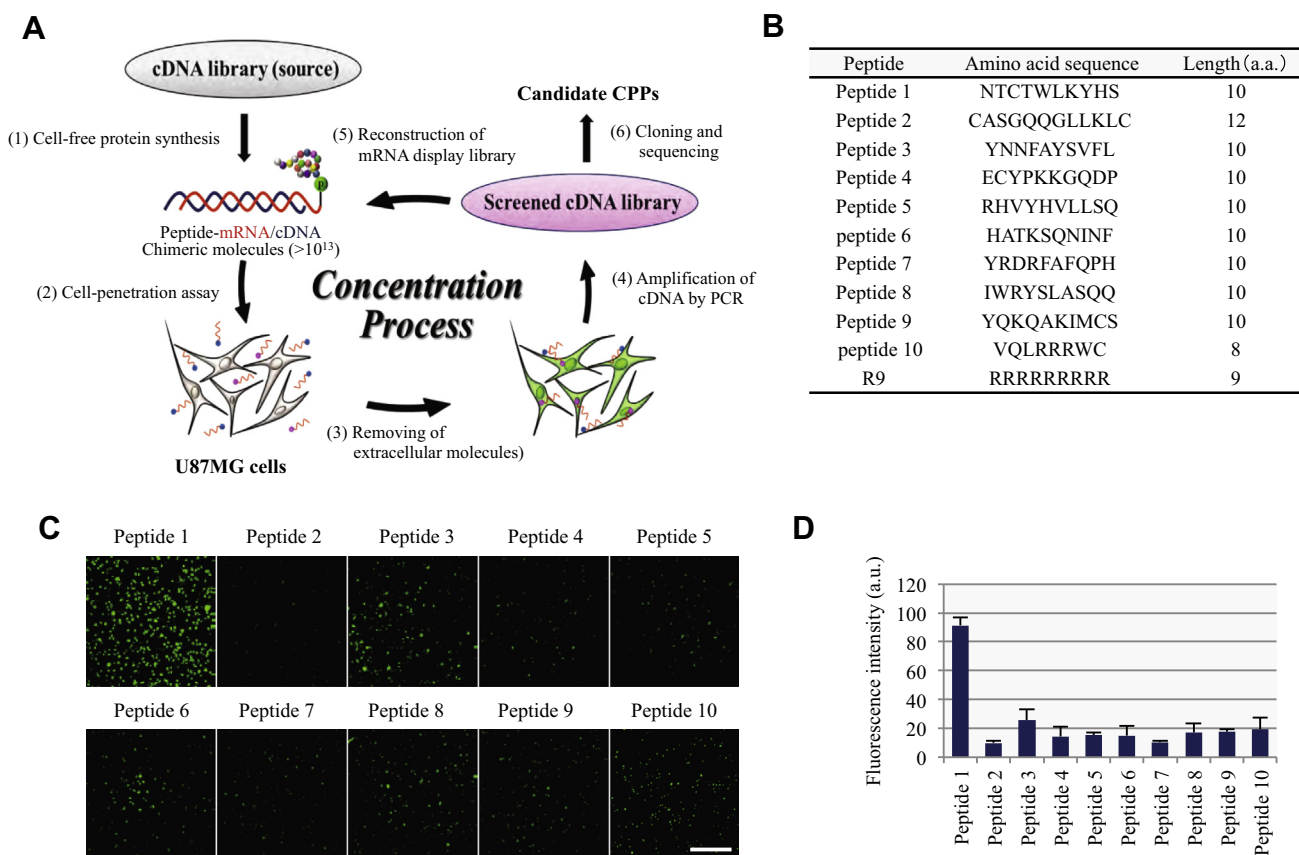


Fig. 1. Screening of candidate CPPs with an affinity for U87MG cells. (A) Scheme of screening for CPPs using mRNA display technology. (1) Construction of mRNA display random peptide libraries in a cell-free translation system. (2) Peptide libraries in the solution were added to the U87MG cell medium. (3) Extracellular peptides were removed by trypsinization and washing. (4) The genomes of chimeric molecules incorporated into the cells were recovered and amplified by their anchored template cDNA using PCR. (5) Reconstruction of mRNA display random peptide libraries for the next selection cycles. (6) After the selection cycles, the peptide sequences of candidate CPPs were predicted by cloning and sequencing. (B) List of peptide sequences selected randomly from the peptides obtained by screening. Poly-arginine (R9) was used as a representative nonselective permeable CPP. (C) U87MG cells were treated with 10 μ M of each numbered FITC-labeled peptide for 2 h at 37 $^{\circ}$ C. Fluorescence images were observed using CLSM. Scale bar, 200 μ m. (D) Meta Morph quantitative analysis of fluorescence intensity of ten candidate CPPs in U87MG cells. The mean fluorescence intensity of the peptides against background was calculated in each image obtained by fluorescence microscopy a.u.; arbitrary unit. Data are presented as the means \pm SD of 3 independent experiments.

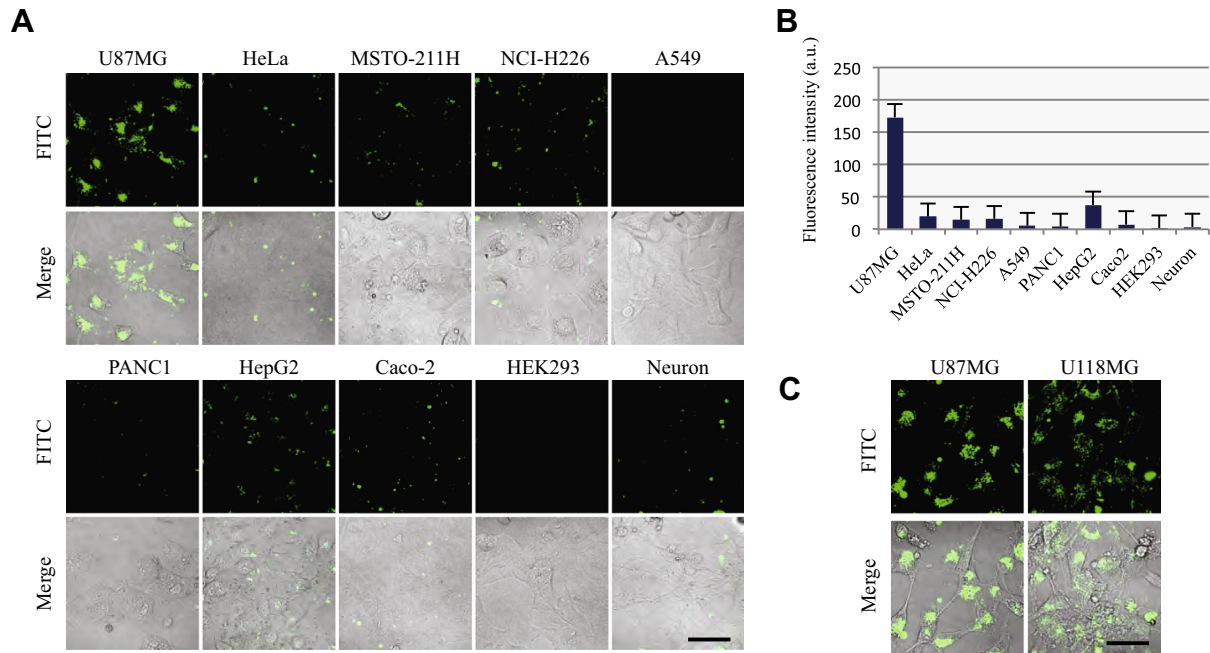


Fig. 2. Cell-penetration assay of peptide1 using cells derived from various tissues. (A) Histologically different cell types were treated with 10 μM of FITC-labeled peptide1 for 2 h at 37 $^{\circ}\text{C}$. Fluorescence images were observed using CLSM. Scale bar, 50 μm . (B) Meta Morph quantitative analysis of fluorescence intensity of peptide1 in cells. The mean fluorescence intensity of peptide1 against background was calculated in each image obtained by fluorescence microscopy a.u.; arbitrary unit. Data are presented as the means \pm SD of 3 independent experiments. (C) Fluorescence images of FITC-labeled peptide1 in U118MG. These cells were treated under the same conditions as mentioned above.

positive control (Fig. 3A). Fluorescence-activated cell sorting (FACS) analysis revealed that intracellular localization of the FITC-labeled peptide1-NSA was 2.0-fold higher than that of peptide1 (Fig. 3B). On the other hand, C3G (NTGTWLKYHS), NTCSA (TWLKYH), and NTHSA (CTWLKY) were decreased. Further, fluorescence images and quantitative analysis showed that peptide1-NSA preserves the permeability into U87MG and U118MG cell lines (Fig. 3C and D). These results suggest that peptide1-NSA has potential as a GBM homing intracellular transporter.

3.4. Antitumor effect of p16 MIS fusion peptide1-NSA against U87MG cells

Deficiency of the p16^{INK4a} tumor suppressor gene is frequently found in the majority of human cancers including GBM [17]. Expression loss of the p16^{INK4a} gene in both U87MG and U118MG cell lines was confirmed by reverse transcription-PCR (Fig. 4A). Therefore, to assess whether peptide1-NSA can deliver cargo into U87MG cells, we focused on a small peptide that comprises the minimal inhibitory sequence of p16 (FLDTLVVLR: p16 MIS), the function of which was described in previous studies [18,19]. The antitumor peptide was designed by fusing peptide1-NSA and p16 MIS (peptide1NSA-p16 MIS) via the Gly-Pro-Gly

spacer, and R4 (RRRR) was tagged at its C-terminus to enhance solubility. Peptide1NSA-p16 V95E, which substitutes valine 95 (V95) in the MIS sequence with glutamate (E), was used as a control (Fig. 4B). U87MG cells were treated with 20 μM of peptide1NSA-p16 MIS or peptide1NSA-p16 V95E for 4 h. After treatment, FACS analysis using Annexin V-FITC and PI (propidium iodide) showed that the early apoptosis rate increased significantly in the p16 MIS conjugate-treated cells ($70 \pm 6.25\%$) compared with p16 V95E conjugate-treated cells ($10 \pm 3.26\%$) and untreated cells ($12 \pm 1.70\%$) (Fig. 4C, right graph). Furthermore, to confirm whether cellular apoptosis was caused by the p16 MIS, we examined the phosphorylation status of retinoblastoma protein (pRB), which is regulated by Cdk4/6, the target for p16^{INK4a}. Twenty-four hours after treatment, western blot analysis revealed that phosphorylated pRB (p-pRB) (Ser^{807/811} phosphorylation) was significantly decreased only in the p16 MIS-treated cells compared with the p16 V95E-treated cells. The p-pRB levels of untreated cells and p16 V95E-treated cells were the same in U87MG cells (Fig. 4D and E). The levels of phosphorylated pRB correlate with the induction of early apoptosis shown in Fig. 4C. These results demonstrated that peptide1-NSA can deliver the p16 functional peptide into U87MG cells as a transporter.

4. Discussion

Targeted cancer therapy holds promise by reducing adverse effects on normal cells and enhancing therapeutic effects [20]. Because CPPs have high biocompatibility and can deliver efficiently a variety of biologically active cargos into cells, studies of cancer-specific drug delivery systems using CPPs have been widely carried out.

In the present study, we report on the GBM selective CPP, peptide1-NSA (TCTWLKYH), which was obtained using mRNA display technology. A protein database search revealed that this peptide appears to encode an artificial sequence, as it has no significant

Table 2

Peptide1-C3G was substituted Cys (C) with Gly (G), and peptide1 deletion series were made by deleting residues from N- and/or C-terminus.

| Peptide | Amino acid sequence | Length (a.a.) |
|-----------------|---------------------|---------------|
| Peptide 1 | NTCTWLKYHS | 10 |
| Peptide 1-C3G | NTGTWLKYHS | 10 |
| Peptide 1-NSA | TCTWLKYHS | 9 |
| Peptide 1-SA | NTCTWLKYH | 9 |
| Peptide 1-NSA | TCTWLKYH | 8 |
| Peptide 1-NTSA | CTWLKYH | 7 |
| Peptide 1-NTCSA | TWLKYH | 6 |
| Peptide 1-NTHSA | CTWLKY | 6 |

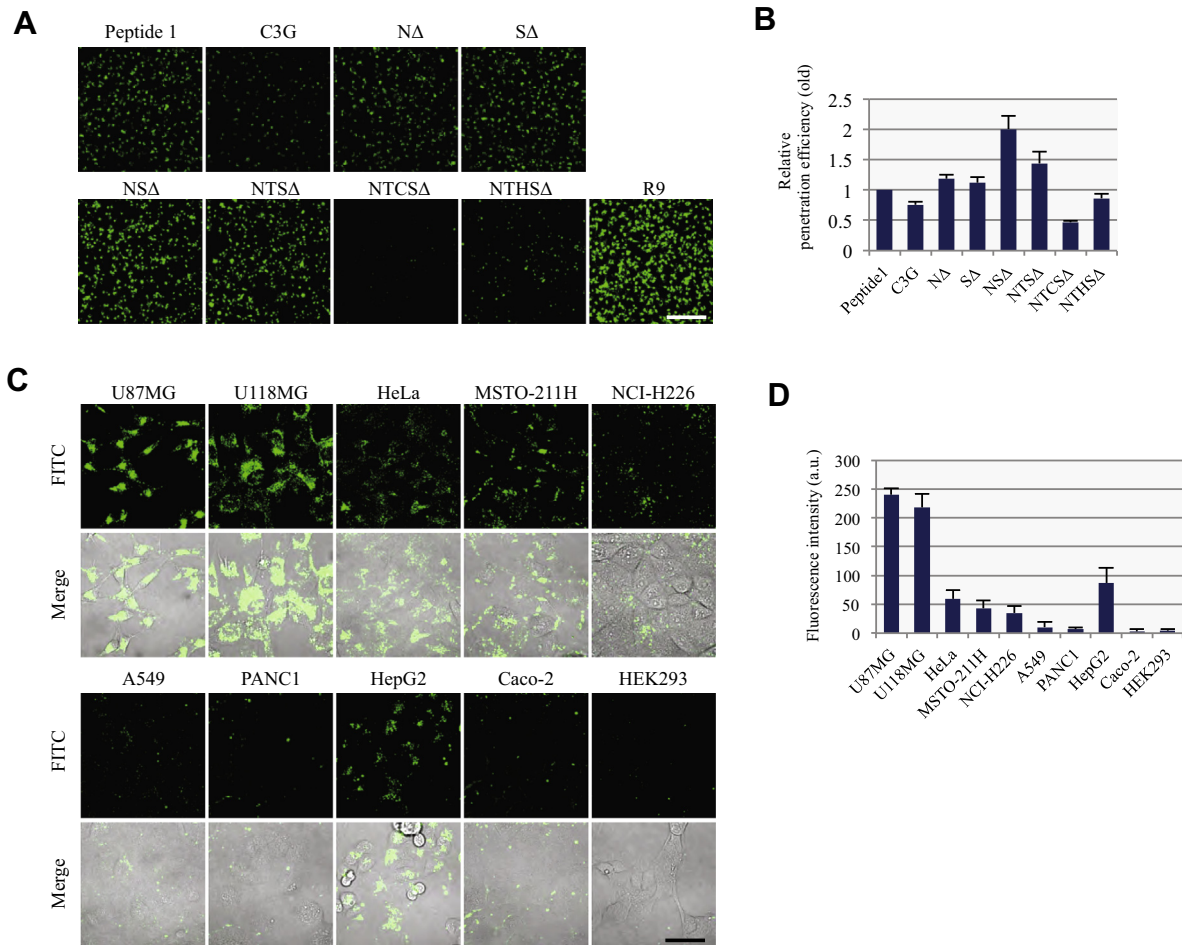


Fig. 3. Analysis of the cell-penetration efficiency of peptide1 variants. (A) U87MG cells were treated with 10 μM of FITC-labeled peptide1 variants for 2 h at 37 $^{\circ}\text{C}$. Fluorescence images were observed using CLSM. Scale bar, 200 μm . (B) FACS quantitative analysis of mean fluorescence intensity of the peptide1 variants in U87MG cells. The relative fluorescence intensity of each peptide compared with peptide1 (1.0) was measured using flow cytometry. Data are presented as means \pm SD of 3 independent experiments. (C) Histologically different cell types were treated with 10 μM of FITC-labeled peptide1-NSA for 2 h at 37 $^{\circ}\text{C}$. Fluorescence images were observed using CLSM. Scale bar, 50 μm . (D) Meta Morph quantitative analysis of fluorescence intensity of peptide1-NSA in cells. The mean fluorescence intensity of peptide1-NSA against background was calculated in each image obtained by fluorescence microscopy a.u.; arbitrary unit. Data are presented as means \pm SD of 3 independent experiments.

identity to any recorded mammalian proteins, including previously reported CPP sequences. The fluorescence-labeled peptide1-NSA was incorporated selectively into U87MG GBM cells *in vitro* (Fig. 3C and D). In most human malignancies, genetic abnormality of tumor suppressor genes has been well characterized [21]. In particular, expressional loss of p16^{INK4a} occurs in U87MG cells (Fig. 4A) [22,23]. The p16^{INK4a} tumor-suppressor gene has been found to be homozygously deleted, mutated or transcriptionally inhibited by methylation in GBMs [24]. p16^{INK4a} binds directly to and inhibits the activity of CDK4 and CDK6, the D-type cyclin-dependent kinases that initiate the phosphorylation of pRB [25], leading to cellular apoptosis and senescence as a result of G1/S phase cell cycle arrest [26]. Analysis of a variety of human cancers has revealed a pattern in the pathway, in which only one of the four members such as cyclin D1, CDK4/CDK6, p16, and pRB of the p16^{INK4a}/CDK/pRB pathway is inactivated [27]. Therefore, restoration of the p16^{INK4a}/CDK/pRB pathway is proposed to be an attractive target for therapeutic intervention because of its important role in cancer development as a cell cycle-regulatory pathway. The peptide1-NSA conjugated p16 MIS functional peptide induced a decrease in the level of phosphorylated pRB and an increase in early cellular apoptosis (Fig. 4C and D). These results suggest that peptide1-NSA can deliver imaging and antitumor agents into U87MG cells as a transporter.

In previous studies, CPPs such as HIV1-TAT and poly-arginine were used as intracellular delivery vehicles in a variety of cell types including peripheral blood lymphocytes, diploid human fibroblasts, keratinocytes, bone marrow stem cells, osteoclasts, fibrosarcoma cells, osteosarcoma, glioma, hepatocellular carcinoma, renal carcinoma, and NIH 3T3 cells (mouse fibroblast-like cell line) [4]. The most important observation in this study is that peptide1-NSA was incorporated selectively into GBM cell lines as compared with other cell lines (Fig. 3C). Although the mechanism responsible for the selective penetration of peptide1-NSA into GBM remains unclear, this unique ability differs notably from the existing CPPs mentioned previously, which enables the targeting function as a GBM-homing peptide.

This study has several limitations. Fluorescence signals of peptide1-NSA were detected at low levels in several cell lines, especially HepG2 and HeLa cells (Fig. 3D). Therefore, these findings may indicate that the level of selectivity requires further improvement in order to warrant designation as a GBM-specific delivery system. Moreover, when we added p16 MIS conjugates to the cell culture medium, aggregates in the medium were observed (data not shown), probably due to the interaction of proteins contained in the medium with the conjugates. This observation indicates that the functionality of this system is likely to be limited by solubility issues. Also, it seems likely that various environmental factors,

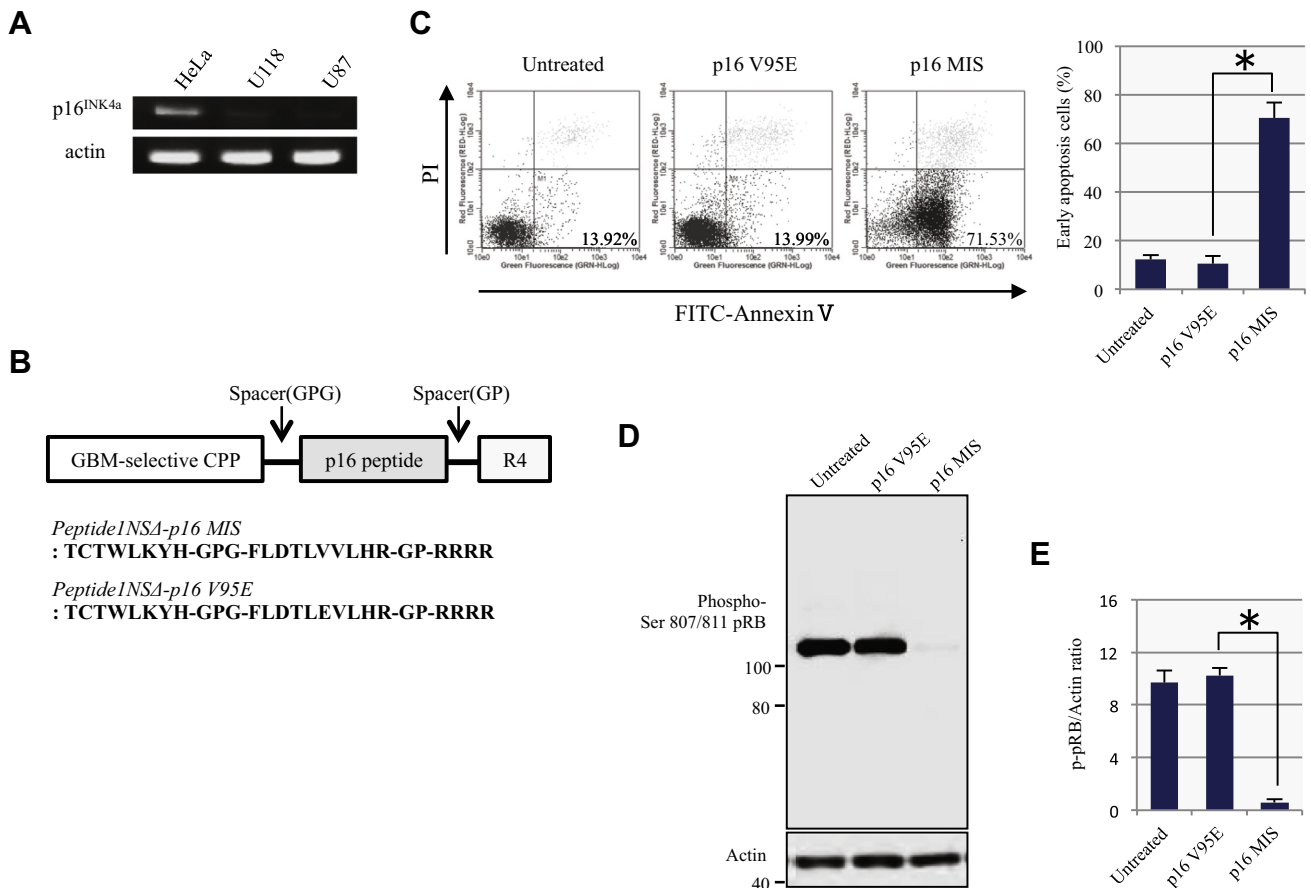


Fig. 4. Therapeutic effect of peptide1NSΔ-p16 MIS conjugates against U87MG cells. (A) RT-PCR analysis of the endogenous mRNA expression of the p16^{INK4a} tumor suppressor gene in two human GBM cells, U87MG and U118MG. HeLa cells were used as a positive control. (B) Design of CPP-p16 antitumor peptide conjugate, which is composed of peptide1-NSA and the functional amino acid sequence of p16^{INK4a} (p16 MIS: minimal inhibitory sequence). p16 V95E was used as a control that substitutes valine 95 (V95) in the MIS sequence with glutamate (E). (C) FACS analysis for cellular apoptosis in U87MG cells treated with 20 μM of peptide1-NSA fused with p16 MIS or p16 V95E for 4 h, respectively. Cells in the lower right quadrant (Annexin V positive/PI negative) represent early apoptotic cells. Percentage of early apoptotic cells (right). Data are presented as the means ± SD of 3 independent experiments per treatment group. (D) Phospho-Ser^{807/811} pRB (p-pRB) status in U87MG cells was assessed by western blotting. Cells were treated with 20 μM of peptide1-NSA fused with p16 MIS or p16 V95E for 24 h, respectively. (E) Ratio of p-pRB/actin of (D). Data are presented as the means ± SD of 3 independent experiments per treatment group. Significant differences of $p < 0.01$ (*) are indicated.

including concentration, treatment time, medium components, and cell sensitivity, are involved in an optimum effect. Thus, further improvement of both the solubility and stability of the p16 MIS conjugate in the medium is needed.

In conclusion, we identified a novel CPP, peptide1-NSΔ, which exhibits selectivity to the U87MG GBM cell line and is capable of delivering its payload into cells *in vitro*. Our findings may provide new avenues for both effective therapeutics and diagnostics in clinical applications as a peptide based delivery system. However, the critical mechanism of tumor selectivity remains to be elucidated. Consequently, further research is required to clarify the GBM-selective recognition mechanisms.

Conflict of interest

The authors disclose no potential conflicts of interest.

Acknowledgments

This research was supported by grants-in-aid for scientific research from the Japanese Ministry of Education, Culture, Sports, Science and Technology (MEXT) (M.M.). This research was also supported by the Uehara Memorial Foundation, Takeda Science Foundation, Special Account Budget for Education and Research

granted from MEXT and The Promotion Project of Medical Clustering of Okinawa prefecture (M.M.).

References

- [1] R. Stupp, W.P. Mason, M.J. van den Bent, M. Weller, B. Fisher, M.J.B. Taphoorn, et al., Radiotherapy plus concomitant and adjuvant temozolomide for glioblastoma, *N. Engl. J. Med.* 352 (2005) 987–996, <http://dx.doi.org/10.1056/NEJMoa043330>.
- [2] J.S. Wadia, S.F. Dowdy, Protein transduction technology, *Curr. Opin. Biotechnol.* 13 (2002) 52–56.
- [3] M.C. Morris, J. Depollier, J. Mery, F. Heitz, G. Divita, A peptide carrier for the delivery of biologically active proteins into mammalian cells, *Nat. Biotechnol.* 19 (2001) 1173–1176, <http://dx.doi.org/10.1038/nbt1201-1173>.
- [4] S.A. Ezhevsky, S.F. Dowdy, H. Hikaru, H. Nagahara, A. Adamina, M. Vocero-Akbani, E. Snyder, Alan Ho, Dawn G. Latham, Natalie A. Lissy, Michelle Becker-Hapak, Transduction of full-length TAT fusion proteins into mammalian cells: TAT-p27 Kip1 induces cell migration, *Nat. Med.* (1998) 1449–1452.
- [5] D. Derossi, A.H. Joliet, G. Chassaing, A. Prochiantz, The third helix of the Antennapedia homeodomain translocates through biological membranes, *J. Biol. Chem.* 269 (1994) 10444–10450.
- [6] S. Futaki, T. Suzuki, W. Ohashi, T. Yagami, S. Tanaka, K. Ueda, et al., Arginine-rich peptides, *J. Biol. Chem.* 276 (2001) 5836–5840, <http://dx.doi.org/10.1074/jbc.M007540200>.
- [7] E. Kondo, M. Seto, K. Yoshikawa, Highly efficient delivery of p16 antitumor peptide into aggressive leukemia / lymphoma cells using a novel transporter system, *Mol. Cancer Ther.* (2005) 1623–1630.
- [8] H. Noguchi, S. Matsumoto, Protein transduction technology: a novel therapeutic perspective, *Acta Med.* Okayama 60 (2006) 1–11.
- [9] E. Koren, V.P. Torchilin, Cell-penetrating peptides: breaking through to the other side, *Trends Mol. Med.* 18 (2012) 385–393.

- [10] S.F.D. Jehangir, S. Wadia, Transmembrane delivery of protein and peptide drugs by TAT-mediated transduction in the treatment of cancer, *Adv. Drug Deliv. Rev.* (2005) 579–596.
- [11] K.J. Lim, B.H. Sung, J.R. Shin, Y.W. Lee, D.J. Kim, K.S. Yang, et al., A cancer specific cell-penetrating peptide, BR2, for the efficient delivery of an scFv into cancer cells, *PLoS ONE* 8 (2013) e66084, <http://dx.doi.org/10.1371/journal.pone.0066084>.
- [12] E. Kondo, K. Saito, Y. Tashiro, K. Kamide, S. Uno, T. Furuya, et al., Tumour lineage-homing cell-penetrating peptides for peptide-based anti-cancer molecular delivery systems, *Nat. Commun.* 951 (2012) 1–13.
- [13] K. Kamide, H. Nakakubo, S. Uno, A. Fukamizu, Isolation of novel cell-penetrating peptides from a random peptide library using in vitro virus and their modifications, *Int. J. Mol. Med.* 25 (2010) 41–51, <http://dx.doi.org/10.3892/ijmm>.
- [14] D. Lipovsek, A. Plu, In-vitro protein evolution by ribosome display and mRNA display, *J. Immunol. Methods* 290 (2004) 51–67, <http://dx.doi.org/10.1016/j.jim.2004.04.008>.
- [15] N. Nemoto, E. Miyamoto-Sato, Y. Husimi, H. Yanagawa, In vitro virus: bonding of mRNA bearing puromycin at the 3'-terminal end to the C-terminal end of its encoded protein on the ribosome in vitro, *FEBS Lett.* 414 (1997) 405–408.
- [16] E. Miyamoto-Sato, M. Ishizaka, K. Horisawa, S. Tateyama, H. Takashima, S. Fuse, et al., Cell-free cotranslation and selection using in vitro virus for high-throughput analysis of protein-protein interactions and complexes, *Genome Res.* 15 (2005) 710–717, <http://dx.doi.org/10.1101/gr.3510505>.
- [17] H. Ohgaki, P. Kleihues, Genetic pathways to primary and secondary glioblastoma, *Am. J. Pathol.* 170 (2007) 1445–1453, <http://dx.doi.org/10.2353/ajpath.2007.070011>.
- [18] K.L. Ball, D.P. Lane, Robin Fahraeus, Sonia Lain, Characterization of the cyclin-dependent kinase inhibitory domain of the INK4 family as a model for a synthetic tumour suppressor molecule, *Oncogene* 16 (1998) 587–596.
- [19] E. Kondo, T. Tanaka, T. Miyake, T. Ichikawa, M. Hirai, M. Adachi, et al., Potent synergy of dual antitumor peptides for growth suppression of human glioblastoma cell lines, *Mol. Cancer Ther.* 7 (2008) 1461–1471, <http://dx.doi.org/10.1158/1535-7163.MCT-07-2010>.
- [20] L. Agemy, D. Friedmann-Morvinski, V.R. Kotamraju, L. Roth, K.N. Sugahara, O.M. Girard, et al., Targeted nanoparticle enhanced proapoptotic peptide as potential therapy for glioblastoma, *Proc. Natl. Acad. Sci. U.S.A.* 108 (2011) 17450–17455, <http://dx.doi.org/10.1073/pnas.1114518108>.
- [21] M. Weller, J. Rieger, C. Grimm, E.G. Van Meir, N. De Tribolet, S. Krajewski, et al., Predicting chemoresistance in human malignant glioma cells: the role of molecular genetic analyses, *Int. J. Cancer* 79 (1998) 640–644.
- [22] J. He, J.J. Olson, C.D. James, C. Lines, Lack of p16 INK4 or retinoblastoma protein (pRb), or amplification-associated overexpression of cdk4 is observed in distinct subsets of malignant glial tumors and cell lines, *Cancer Res.* 55 (1995) 4833–4836.
- [23] F.D. Ragione, G.L. Russo, A. Oliva, C. Mercurio, S. Mastropietro, V.D. Pietra, et al., Biochemical characterization of p16INK4- and p18-containing complexes in human cell lines, *J. Biol. Chem.* 271 (1996) 15942–15949, <http://dx.doi.org/10.1074/jbc.271.27.15942>.
- [24] M.A. Al-Mohanna, P.S. Manogaran, Z. Al-Mukhalafi, K. A Al-Hussein, A. Aboussekhra, The tumor suppressor p16(INK4a) gene is a regulator of apoptosis induced by ultraviolet light and cisplatin, *Oncogene* 23 (2004) 201–212, <http://dx.doi.org/10.1038/sj.onc.1206927>.
- [25] J. Calbó, M. Marotta, M. Cascalló, J.M. Roig, J.L. Gelpí, J. Fueyo, et al., Adenovirus-mediated wt-p16 reintroduction induces cell cycle arrest or apoptosis in pancreatic cancer, *Cancer Gene Ther.* 8 (2001) 740–750, <http://dx.doi.org/10.1038/sj.cgt.7700374>.
- [26] K. Zennami, K. Yoshikawa, E. Kondo, K. Nakamura, Y. Upsilonamada, M.A. De Velasco, et al., A new molecular targeted therapeutic approach for renal cell carcinoma with a p16 functional peptide using a novel transporter system, *Oncol. Rep.* 26 (2011) 327–333, <http://dx.doi.org/10.3892/or.2011.1290>.
- [27] K. Fujimoto, R. Hosotani, Y. Miyamoto, R. Doi, T. Koshiba, A. Otaka, et al., Inhibition of pRb phosphorylation and cell cycle progression by an antennapedia-p16(INK4A) fusion peptide in pancreatic cancer cells, *Cancer Lett.* 159 (2000) 151–158.



Original article

Development of an experimentally useful model of acute myocardial infarction: 2/3 nephrectomized triple nitric oxide synthases-deficient mouse



Taro Uchida ^{a,1}, Yumi Furuno ^{b,1}, Akihide Tanimoto ^c, Yumiko Toyohira ^d, Kumiko Arakaki ^e, Mika Kina-Tanada ^a, Haruaki Kubota ^a, Mayuko Sakanashi ^a, Toshihiro Matsuzaki ^a, Katsuhiko Noguchi ^a, Junko Nakasone ^a, Tomonori Igarashi ^f, Susumu Ueno ^f, Masayuki Matsushita ^g, Shogo Ishiuchi ^h, Hiroaki Masuzaki ⁱ, Yusuke Ohya ^e, Nobuyuki Yanagihara ^d, Hiroaki Shimokawa ^j, Yutaka Otsuji ^b, Masahito Tamura ^b, Masato Tsutsui ^{a,*}

^a Department of Pharmacology, Graduate School of Medicine, University of the Ryukyus, Okinawa, Japan

^b Second Department of Internal Medicine, School of Medicine, Institute of Industrial Ecological Sciences, University of Occupational and Environmental Health, Kitakyushu, Japan

^c Department of Pathology, Kagoshima University Graduate School of Medical and Dental Sciences, Kagoshima, Japan

^d Department of Pharmacology, School of Medicine, Institute of Industrial Ecological Sciences, University of Occupational and Environmental Health, Kitakyushu, Japan

^e Third Department of Internal Medicine, Graduate School of Medicine, University of the Ryukyus, Okinawa, Japan

^f Department of Occupational Toxicology, Institute of Industrial Ecological Sciences, University of Occupational and Environmental Health, Kitakyushu, Japan

^g Department of Physiology, Graduate School of Medicine, University of the Ryukyus, Okinawa, Japan

^h Department of Neurosurgery, Graduate School of Medicine, University of the Ryukyus, Okinawa, Japan

ⁱ Second Department of Internal Medicine, Graduate School of Medicine, University of the Ryukyus, Okinawa, Japan

^j Department of Cardiovascular Medicine, Tohoku University Graduate School of Medicine, Sendai, Japan

ARTICLE INFO

Article history:

Received 23 July 2014

Received in revised form 9 September 2014

Accepted 17 September 2014

Available online 28 September 2014

Keywords:

Arteriosclerosis

Acute myocardial infarction

Nitric oxide synthase

Sudden cardiac death

ABSTRACT

We investigated the effect of subtotal nephrectomy on the incidence of acute myocardial infarction (AMI) in mice deficient in all three nitric oxide synthases (NOSs). Two-thirds nephrectomy (NX) was performed on male triple NOSs^{-/-} mice. The 2/3NX caused sudden cardiac death due to AMI in the triple NOSs^{-/-} mice as early as 4 months after the surgery. The 2/3NX triple NOSs^{-/-} mice exhibited electrocardiographic ST-segment elevation, reduced heart rate variability, echocardiographic regional wall motion abnormality, and accelerated coronary arteriosclerotic lesion formation. Cardiovascular risk factors (hypertension, hypercholesterolemia, and hyperglycemia), an increased number of circulating bone marrow-derived vascular smooth muscle cell (VSMC) progenitor cells (a pro-arteriosclerotic factor), and cardiac up-regulation of stromal cell-derived factor (SDF)-1 α (a chemotactic factor of the progenitor cells) were noted in the 2/3NX triple NOSs^{-/-} mice and were associated with significant increases in plasma angiotensin II levels (a marker of renin–angiotensin system activation) and urinary 8-isoprostane levels (a marker of oxidative stress). Importantly, combined treatment with a clinical dosage of an angiotensin II type 1 receptor blocker, irbesartan, and a calcium channel antagonist, amlodipine, markedly prevented coronary arteriosclerotic lesion formation and the incidence of AMI and improved the prognosis of those mice, along with ameliorating all those pro-arteriosclerotic parameters. The 2/3NX triple NOSs^{-/-} mouse is a new experimentally useful model of AMI. Renin–angiotensin system activation, oxidative stress, cardiovascular risk factors, and SDF-1 α -induced recruitment of bone marrow-derived VSMC progenitor cells appear to be involved in the pathogenesis of AMI in this model.

© 2014 Elsevier Ltd. All rights reserved.

Abbreviations: ACE, angiotensin-converting enzyme; ADMA, asymmetric dimethyl-arginine; AMI, acute myocardial infarction; APC, activated protein C; apo E, apolipoprotein E; AT₁, angiotensin II type 1; CKD, chronic kidney disease; ECG, electrocardiography; FITC, fluorescein isothiocyanate; GAPDH, glyceraldehyde-3-phosphate dehydrogenase; HDL, high-density lipoprotein; mAb, monoclonal antibody; NO, nitric oxide; NOS, NO synthase; NX, nephrectomy; Sca-1⁺, stem cell antigen-1⁺; SDF-1 α , stromal cell-derived factor-1 α ; VSMC, vascular smooth muscle cell; WHHL, Watanabe heritable hyperlipidemic; WT, wild-type.

* Corresponding author at: Department of Pharmacology, Graduate School of Medicine, University of the Ryukyus, 207 Uehara, Nishihara, Okinawa 903-0215, Japan. Tel.: +81 98 895 1133; fax: +81 98 895 1411.

E-mail address: tsutsui@med.u-ryukyu.ac.jp (M. Tsutsui).

¹ These authors contributed equally to this work.

1. Introduction

Acute myocardial infarction is a disorder in which cardiac myocytes undergo necrosis as a consequence of interrupted coronary blood flow [1]. Acute myocardial infarction is a major cause of morbidity and mortality worldwide, with more than 7 million people in the world suffering from acute myocardial infarction each year [1]. Over the past two decades, the in-hospital mortality rate after admission for acute myocardial infarction has substantially declined to less than 10%, owing to

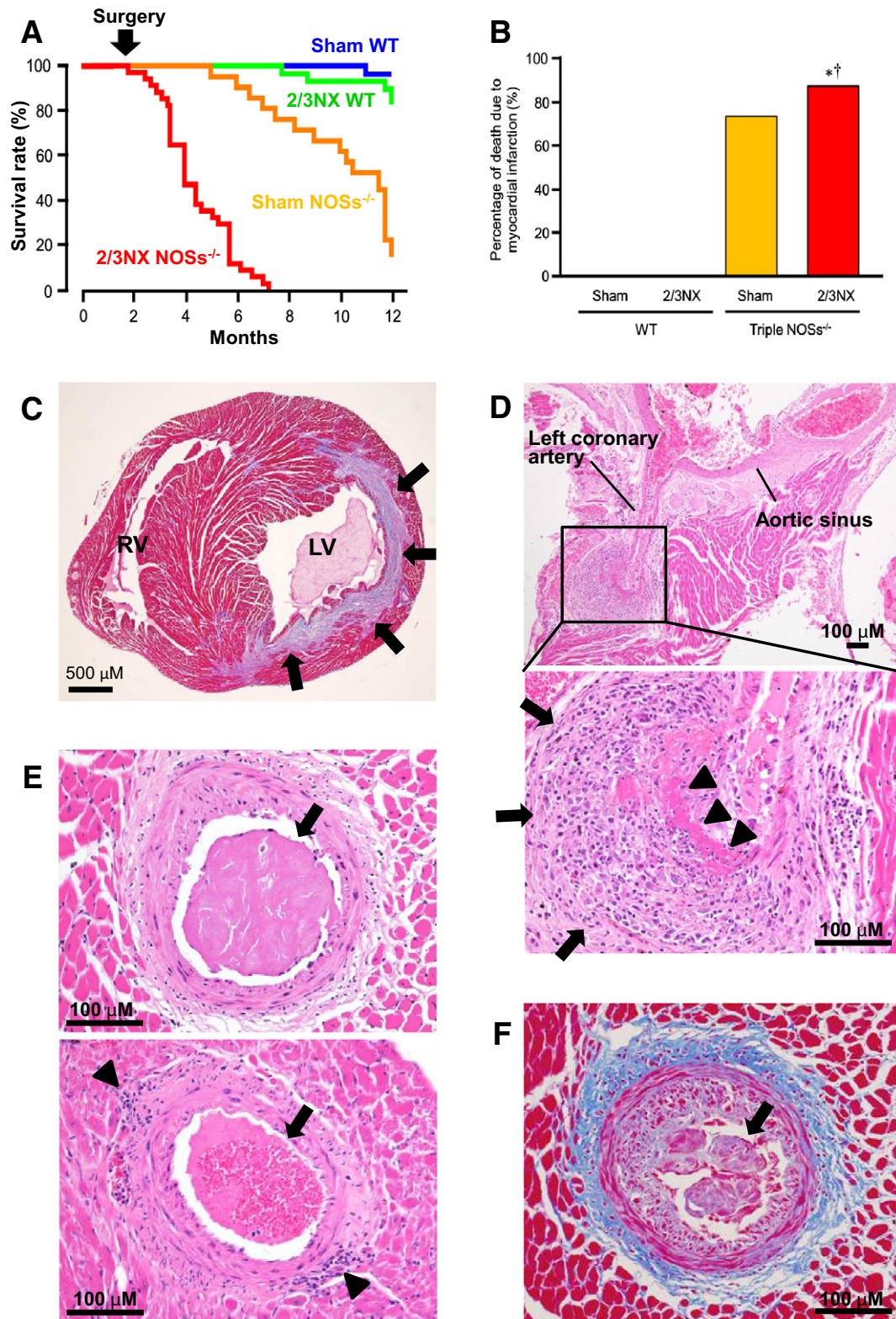


Fig. 1. Sudden cardiac death due to spontaneous myocardial infarction in 2/3 nephrectomized (NX) male triple nitric oxide synthases (NOSs)-deficient mice. (A) Survival rate ($n = 28-49$). NOSs^{-/-}, triple NOSs^{-/-} mice; WT, wild-type mice; sham, sham-operated. (B) Percentage of death due to myocardial infarction in the total causes of death ($n = 2-32$). Sham, sham operation. (C) Lateral wall myocardial infarction (arrows) (Azán staining). LV, left ventricle; RV, right ventricle. (D) Marked infiltration of inflammatory cells (arrows) and fibrinoid necrosis (triangles) at the adventitia of the left coronary artery (hematoxylin-eosin staining). (E) Intracoronary thrombi (arrows) and adventitial infiltration of inflammatory cells (triangles) (hematoxylin-eosin staining). (F) Intimal thickening, perivascular fibrosis (blue color), and intracoronary thrombus (arrow) (Azán staining).

recent therapeutic advances such as coronary reperfusion therapy [2]. However, the overall mortality rate, including out-of-hospital deaths, is very high (approximately 30%) even at present [3]. This is because the majority of these deaths occur before stricken individuals reach the hospital [3]. Outside the hospital, once the individuals develop severe complications, such as malignant cardiac arrhythmia, cardiogenic shock, or cardiac rupture, it is extremely difficult to save their lives [3]. Thus, in order to suppress this fatal cardiovascular disorder, research and development of therapeutic strategies for preventing acute myocardial infarction are of critical importance. However, due to lack of an experimentally useful animal model that develops acute myocardial infarction, the research and development of such strategies have made little progress.

Nitric oxide (NO) plays an essential role in maintaining cardiovascular homeostasis. NO is synthesized by three distinct NO synthase (NOS) isoforms, including neuronal, inducible, and endothelial NOSs, and exerts a variety of biological actions under both physiological and

pathological conditions [4–9]. We previously generated mice in which all three NOS genes are completely disrupted [10] and reported that triple NOS^{-/-} mice, but not single endothelial NOS^{-/-} mice, spontaneously emerge acute myocardial infarction [11]. However, our model was not useful for experiments because it took a very long time (approximately 1 year) for them to develop acute myocardial infarction [11].

Chronic kidney disease (CKD) is a condition characterized by progressive and irreversible loss of renal function. It is estimated that over 10% of the adult population in developed countries suffer some degree of CKD [12,13]. Previous epidemiological studies have indicated that the presence of CKD significantly increases the risk of acute myocardial infarction in men, and that the impact of CKD on the risk of cardiovascular disease is as strong as that of diabetes mellitus and pre-existing ischemic heart disease [14–16]. In the clinical course of the progression of CKD, the number of nephrons decreases regardless of etiology, and this pathological renal remodeling is thought to be the final common

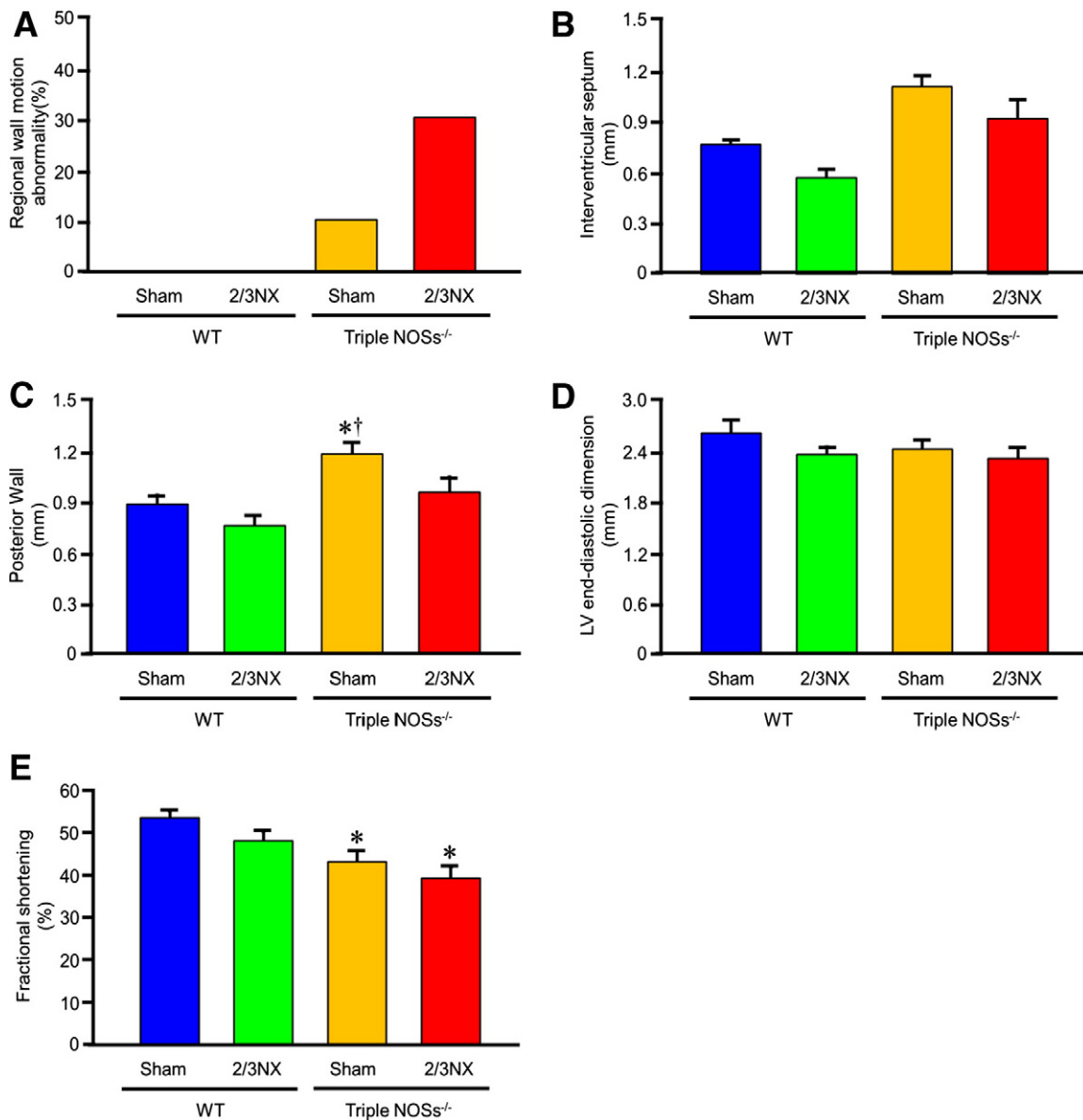


Fig. 2. Echocardiographic abnormalities in 2/3NX triple NOSs^{-/-} mice at 2 months after the surgery. (A) Regional wall motion abnormality ($n = 10$). NOSs^{-/-}, triple NOSs^{-/-} mice; WT, wild-type mice; sham, sham-operated. (B) Wall thickness of interventricular septum ($n = 10$). (C) Wall thickness of posterior wall ($n = 10$). (D) Left ventricular (LV) end-diastolic dimension ($n = 10$). (E) Fractional shortening ($n = 10$).

pathway in the pathogenesis of CKD. Such a disease state is modeled in experimental animals by surgically dissecting a large part of the renal mass [17,18].

In the present study, based on these backgrounds, we investigated the effect of subtotal nephrectomy on the incidence of acute myocardial infarction in our male triple NOSs^{-/-} mice in order to establish an experimentally useful model of acute myocardial infarction.

2. Materials and methods

Materials and methods are described in the online Supplementary Methods and Results.

3. Results

3.1. Subtotal 2/3 nephrectomy (NX) caused an early onset of acute myocardial infarction in male triple NOSs^{-/-} mice

Because animals with 5/6NX are widely used as an experimental model of CKD, we first studied the effect of 5/6NX on survival rate in male triple NOSs^{-/-} mice. However, almost all the triple NOSs^{-/-} mice died shortly after the 5/6NX (data not shown). Thus, we next examined the effect of 2/3NX. In male wild-type (WT) mice, the 2/3NX did not significantly affect the survival rate as compared with sham operation, and more than 80% of the 2/3NX WT mice lived during the 10 months of follow-up (Fig. 1A). In contrast,

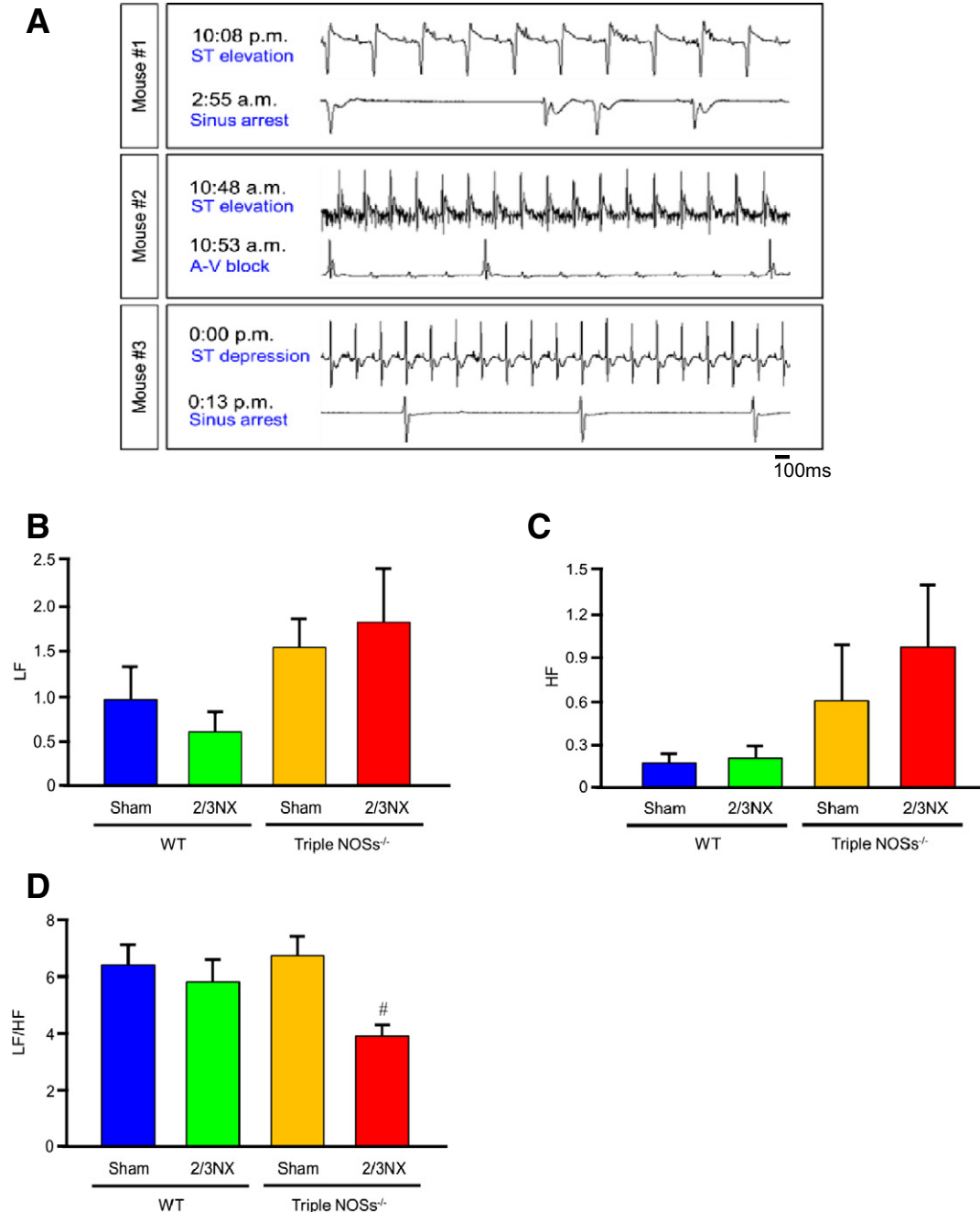


Fig. 3. Telemetry electrocardiographic abnormalities in 2/3NX triple NOSs^{-/-} mice at 2 months after the surgery. (A) Electrocardiographic (ECG) abnormalities in 3 2/3NX triple NOSs^{-/-} mice that died during ECG recording (died within 24 hours after subcutaneous implantation of telemetry transmitters). A-V, atrioventricular. (B) Low-frequency (LF) power ($n = 10-12$). (C) High-frequency (HF) power ($n = 10-12$). (D) LF/HF ratio ($n = 10-12$). * $P < 0.05$ vs. sham-operated WT mice; [#] $P < 0.05$ vs. sham-operated triple NOSs^{-/-} mice.

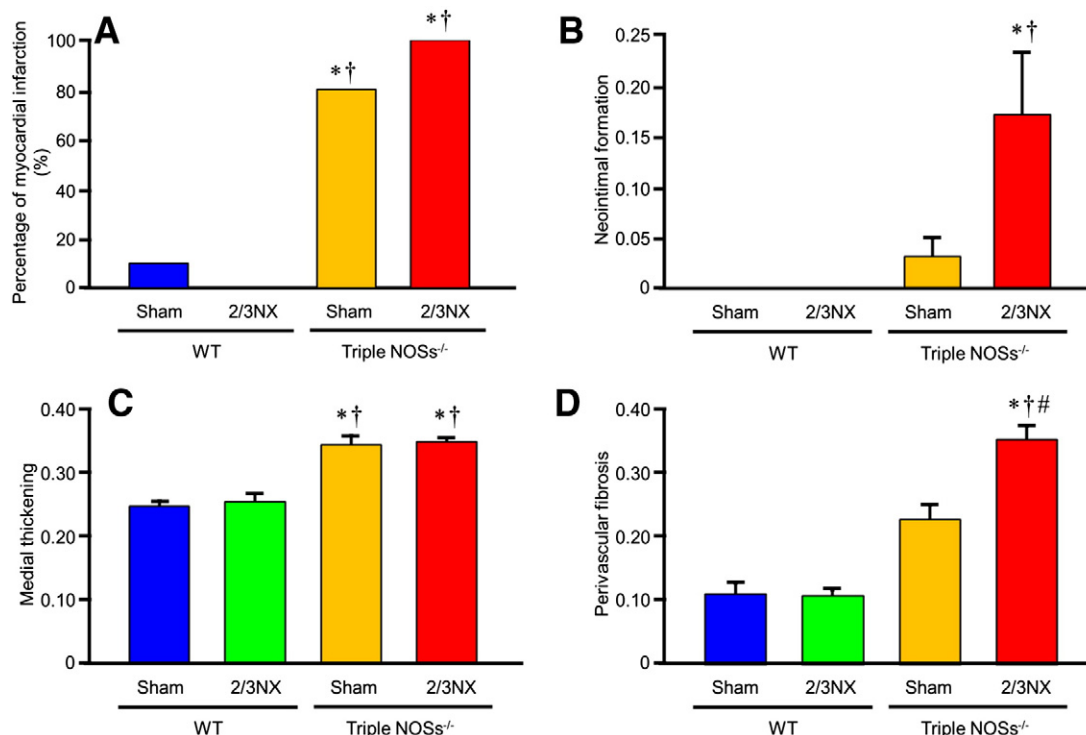


Fig. 4. Coronary arteriosclerotic lesion formation in 2/3NX triple NOSs^{-/-} mice at 2 months after the surgery. After the echocardiography and telemetry ECG, pathological examination of the heart was performed. Four 2/3NX triple NOSs^{-/-} mice that died before 2 months after the surgery and 3 2/3NX triple NOSs^{-/-} mice that died during telemetry ECG were included in the analysis. The heart was cut into 5 equal-thick parts in a short-axis direction, and respective 5 sections were examined. (A) Percentage of acute and/or old myocardial infarction ($n = 10-16$). NOSs^{-/-}, triple NOSs^{-/-} mice; WT, wild-type mice; sham, sham-operated. (B) Neointimal formation (the ratio of intima area to media area) ($n = 10-16$). (C) Medial thickening (the ratio of media area to total vascular area) ($n = 10-16$). (D) Perivascular fibrosis (the ratio of perivascular area to total vascular area) ($n = 10-16$). * $P < 0.05$ vs. sham-operated WT mice; † $P < 0.05$ vs. 2/3NX WT mice; # $P < 0.05$ vs. sham-operated triple NOSs^{-/-} mice.

in the triple NOSs^{-/-} mice, the 2/3NX significantly and markedly reduced the survival rate compared with sham operation, and, importantly, approximately 90% of the 2/3NX triple NOSs^{-/-} mice suddenly died as early as 4 months after the surgery (Fig. 1A).

We next explored the effect of 2/3NX on the incidence of acute myocardial infarction in the triple NOSs^{-/-} mice by a postmortem examination, which revealed a marked increase in the incidence of myocardial infarction (the percentage of death due to myocardial infarction in the total causes of death) compared with sham operation. Noticeably, 87.8% (43/49) of the 2/3NX triple NOSs^{-/-} mice died due to acute and/or old myocardial infarction (Fig. 1B). It was conceivable that the 2/3NX triple NOSs^{-/-} mice would die mainly due to myocardial infarction-complicated arrhythmias or heart failure (including cardiogenic shock). It is difficult to distinguish between death due to arrhythmias and heart failure since heart failure is often accompanied by arrhythmias and since arrhythmias are always seen prior to any death. Thus, we categorized those causes of death as death due to myocardial infarction. No cerebrovascular disease was observed in any of the dead 2/3NX triple NOSs^{-/-} mice. Fig. 1C represents the lateral wall myocardial infarction seen in the dead 2/3NX triple NOSs^{-/-} mice. The coronary arteries of the dead 2/3NX triple NOSs^{-/-} mice exhibited severe coronary arteriosclerotic lesion formation, including infiltration of inflammatory cells (Fig. 1D), neointimal formation (Fig. 1F), medial thickening (Fig. 1F), perivascular fibrosis (Fig. 1F), and fibrinoid necrosis (Fig. 1D), as well as coronary thrombus formation (Figs. 1E, F). On the other hand, coronary atherosclerotic lesions, such as extracellular lipid accumulation, atheromatous plaque formation, or infiltration of foamy macrophages in the coronary artery, were rarely observed.

3.2. 2/3NX caused echocardiographic and electrocardiographic abnormalities and accelerated coronary arteriosclerotic lesion formation in triple NOSs^{-/-} mice at 2 months after the surgery

We then examined cardiac functional abnormalities and the extent of coronary arteriosclerotic lesion formation in the 2/3NX triple NOSs^{-/-} mice at 2 months post-surgery via echocardiography, telemetry electrocardiography (ECG), and pathological examination. Of the 16 2/3NX triple NOSs^{-/-} mice, 4 died before 2 months after the surgery. Echocardiography showed regional wall motion abnormality in 30% (3/10) of the 2/3NX triple NOSs^{-/-} mice and 10% (1/10) of the sham triple NOSs^{-/-} mice (Fig. 2A). Wall thickness of interventricular septum and posterior wall tended to be thinner and fractional shortening tended to be more reduced in the 2/3NX triple NOSs^{-/-} mice as compared with the sham triple NOSs^{-/-} mice, and fractional shortening was significantly decreased in the 2/3NX triple NOSs^{-/-} mice when compared with the sham WT mice (Figs. 2B, C, E). There was no significant difference in left ventricular end-diastolic dimension between the 2/3NX triple NOSs^{-/-} mice and other mice (Fig. 2D).

Of the 12 2/3NX triple NOSs^{-/-} mice that received subcutaneous implantation of telemetry transmitters, 3 died during ECG recording (within 24 hours after the implantation), and ECG revealed ST-segment elevation followed by sinus arrest, ST-segment elevation followed by advanced atrioventricular block, and ST-segment depression followed by sinus arrest (Fig. 3A). Transient ST-segment depression was detected in other 2 2/3NX triple NOSs^{-/-} mice and 1 sham triple NOSs^{-/-} mice. No ischemic ECG change was seen in sham or 2/3NX WT mice. We evaluated heart rate variability parameters, such as low-frequency (LF) power, high-frequency (HF) power, and LF/HF ratio.

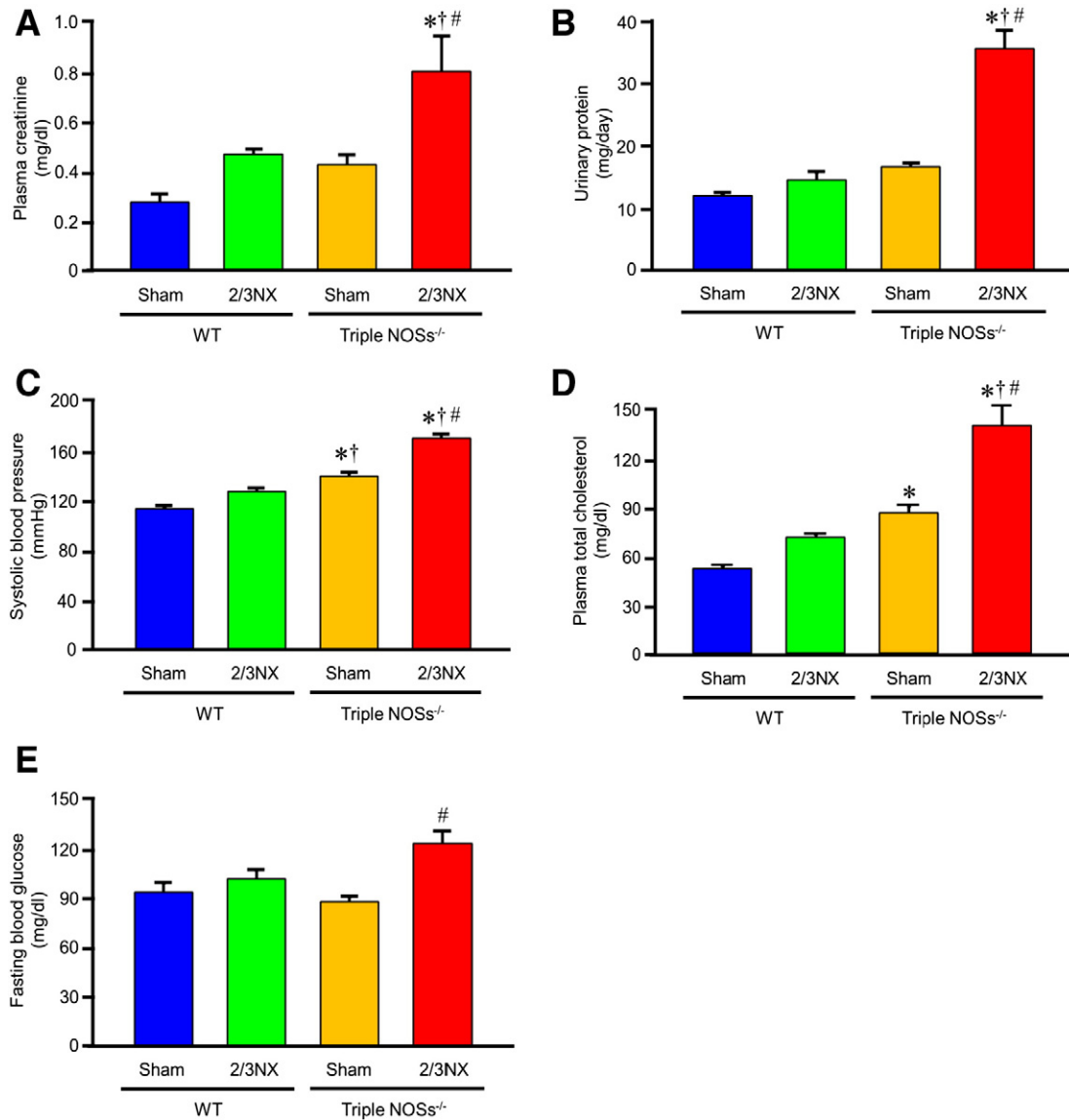


Fig. 5. Renal dysfunction and cardiovascular risk factors in the 2/3NX triple NOSs^{-/-} mice. These parameters were assessed at 2 months after the surgery. (A) Plasma creatinine levels ($n = 10$). (B) Urinary protein levels ($n = 12$). (C) Systolic blood pressure ($n = 12$). (D) Plasma total cholesterol levels ($n = 10$). (E) Fasting blood glucose levels ($n = 10$). * $P < 0.05$ vs. sham-operated WT mice; † $P < 0.05$ vs. 2/3NX WT mice; # $P < 0.05$ vs. sham-operated triple NOSs^{-/-} mice.

The LF power and the HF power tended to be increased in the 2/3NX triple NOSs^{-/-} mice, and the LF/HF ratio was significantly decreased in the 2/3NX triple NOSs^{-/-} mice as compared with the sham NOSs^{-/-} mice (Figs. 3B–D).

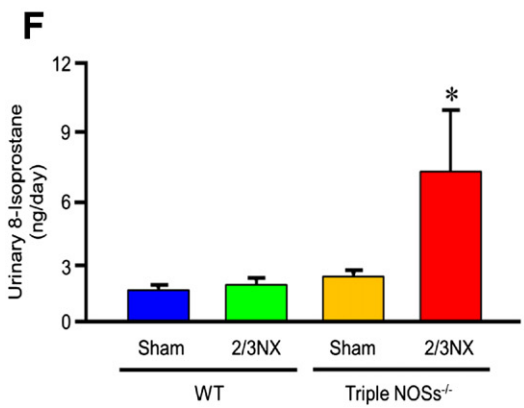
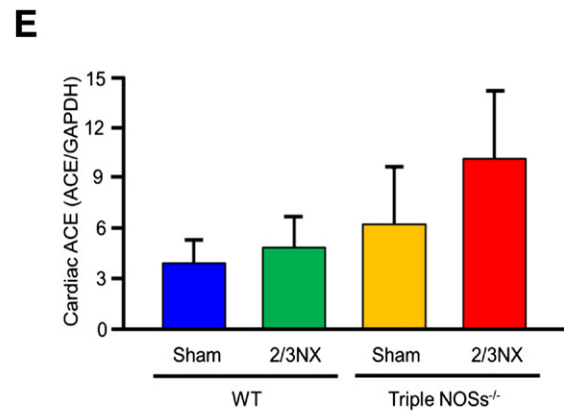
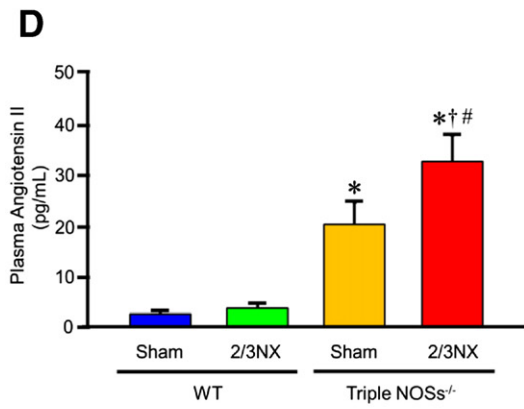
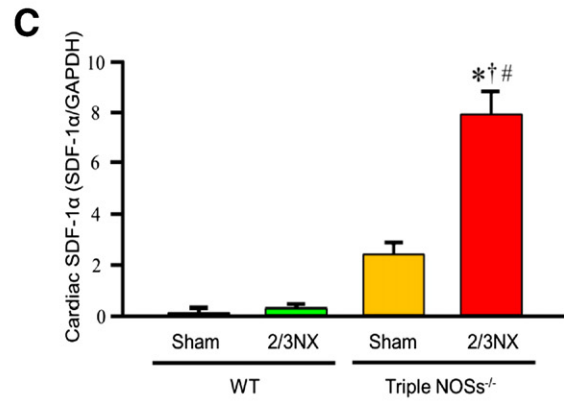
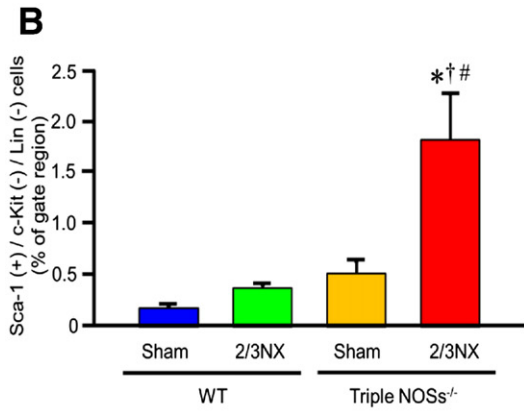
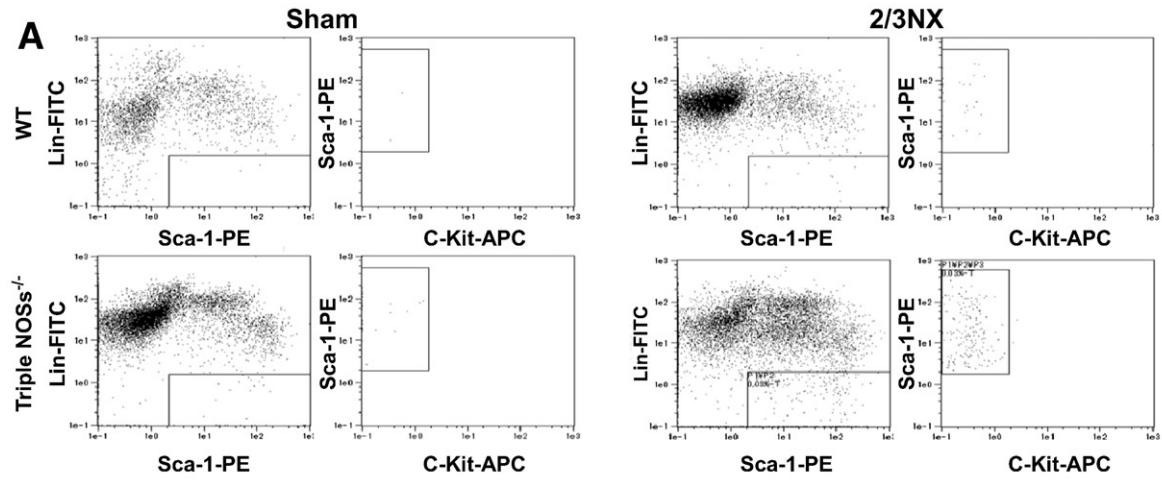
After echocardiography and telemetry ECG, we quantitated the extent of coronary arteriosclerosis. Four 2/3NX triple NOSs^{-/-} mice that died before 2 months after the surgery and 3 2/3NX triple NOSs^{-/-} mice that died during telemetry ECG were included in the analysis. The heart was cut into 5 equal-thick parts in a short-axis direction, and respective 5 sections were examined. Acute and/or old myocardial infarction was recognized in 100% (16/16) of the 2/3NX triple NOSs^{-/-} mice and 80% (8/10) of the sham triple NOSs^{-/-} mice

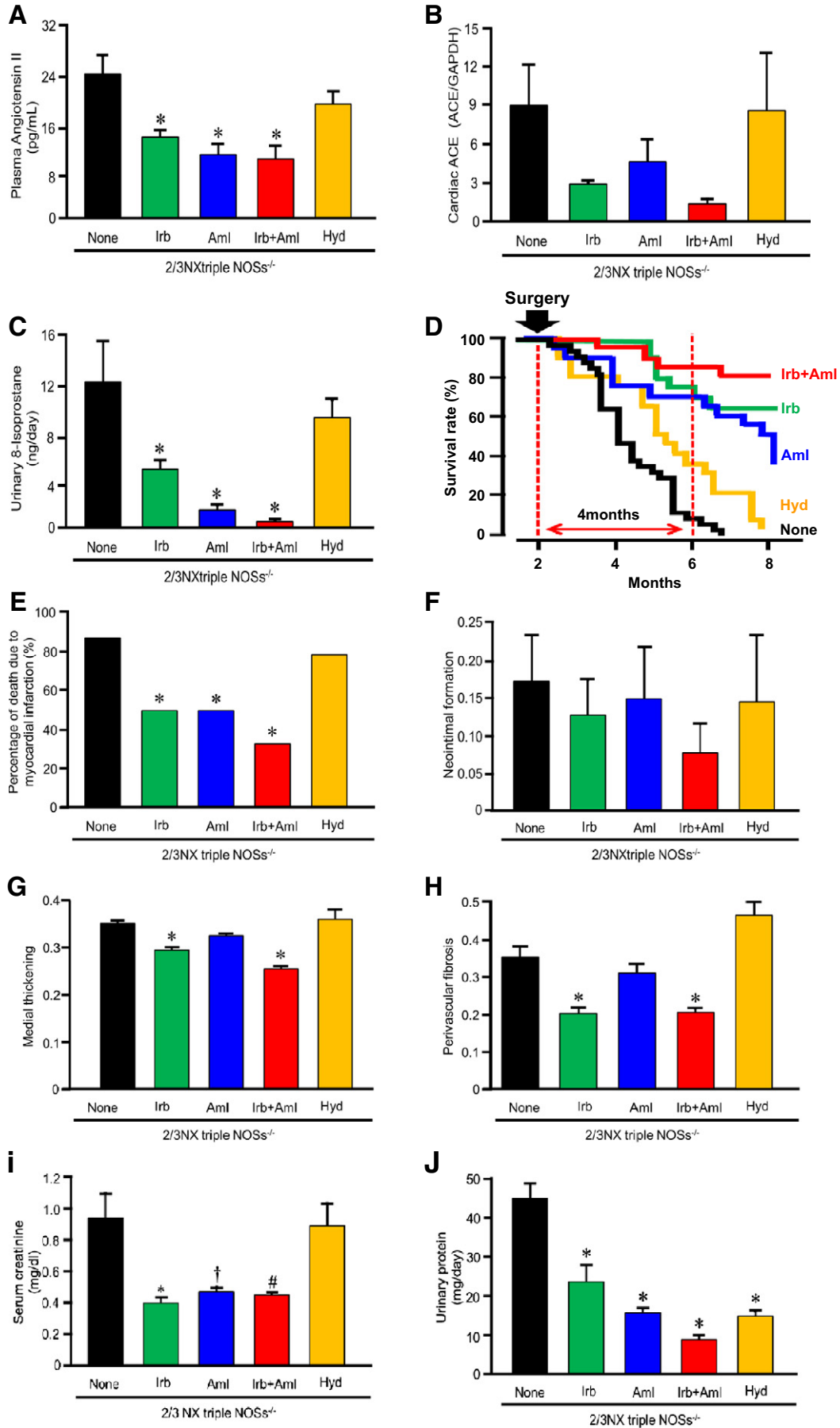
(Fig. 4A). The extents of neointimal formation, medial thickening, and perivascular fibrosis were all markedly accelerated in the 2/3NX triple NOSs^{-/-} mice as compared with the sham WT mice (Figs. 4B–D). Coronary thrombus formation was also noted in 1 2/3NX triple NOSs^{-/-} mice.

3.3. 2/3NX reduced renal function in triple NOSs^{-/-} mice

There were significant increases in plasma creatinine and urinary protein levels, markers of renal function, after the 2/3NX (assessed at 2 months after the surgery) in the triple NOSs^{-/-} mice compared with sham operation (Figs. 5A, B).

Fig. 6. Stromal cell-derived factor (SDF)-1 α -induced recruitment of circulating bone marrow-derived vascular smooth muscle cell (VSMC) progenitor cells, renin-angiotensin system activation, and oxidative stress in the 2/3NX triple NOS^{-/-} mice. (A and B) The number of circulating stem cell antigen-1⁺ (Sca-1⁺)/c-Kit⁻/Lin⁻ cells (interpreted as bone marrow-derived VSMC progenitor cells) analyzed at 1 week after the surgery ($n = 7$). (C) Cardiac SDF-1 α protein levels assayed at 1 week after the surgery ($n = 4-6$). (D) Plasma angiotensin II levels measured at 2 months after the surgery ($n = 8$). (E) Cardiac angiotensin-converting enzyme (ACE) protein expression levels evaluated at 2 months after the surgery ($n = 7$). (F) Urinary 8-isoprostane levels assessed at 2 months after the surgery ($n = 8$). * $P < 0.05$ vs. sham-operated WT mice; † $P < 0.05$ vs. 2/3NX WT mice; # $P < 0.05$ vs. sham-operated triple NOSs^{-/-} mice.





3.4. 2/3NX exacerbated cardiovascular risk factors in triple NOSs^{-/-} mice

Because severe coronary arteriosclerotic lesions were detected in the 2/3NX triple NOSs^{-/-} mice, we then examined the presence or absence of cardiovascular risk factors. The 2/3NX caused significant increases in systolic blood pressure (measured at 1 month after the surgery), plasma total cholesterol levels, and fasting blood glucose levels (evaluated at 2 months after the surgery) in the triple NOSs^{-/-} mice compared with sham operation (Figs. 5C–E).

3.5. 2/3NX caused mobilization of circulating bone marrow-derived vascular smooth muscle cell (VSMC) progenitor cells and up-regulation of cardiac stromal cell-derived factor 1 α (SDF-1 α) levels in triple NOSs^{-/-} mice

It has been reported that bone marrow-derived VSMC progenitor cells contribute to arteriosclerotic lesion formation after vascular injury and that SDF-1 α recruits the VSMC progenitor cells to vascular lesions [19]. We thus analyzed the effects of 2/3NX on the number of circulating bone marrow-derived VSMC progenitor cells and cardiac SDF-1 α protein levels in the triple NOSs^{-/-} mice. The 2/3NX significantly and markedly augmented the number of circulating stem cell antigen-1⁺ (Sca-1⁺)/c-Kit⁻/Lin⁻ cells, which are interpreted as bone marrow-derived VSMC progenitor cells (evaluated at 1 week after the surgery), and the cardiac SDF-1 α protein levels (assayed at 1 week after the surgery) in the triple NOSs^{-/-} mice compared with sham operation (Figs. 6A–C and Online Supplementary Fig. 1).

3.6. 2/3NX caused renin–angiotensin system activation and oxidative stress in triple NOSs^{-/-} mice

We next investigated the molecular mechanisms for acute myocardial infarction caused by the 2/3NX in the triple NOSs^{-/-} mice. The 2/3NX evoked prominent increases in plasma angiotensin II levels and cardiac angiotensin-converting enzyme (ACE) protein levels, markers of renin–angiotensin system activation (assessed at 2 months after the surgery) in the triple NOSs^{-/-} mice compared with sham operation (Figs. 6D and E, and Online Supplementary Fig. 2), although the values of the cardiac ACE protein levels did not reach a statistically significant level because of variations in the data. The 2/3NX also elicited a marked rise in urinary 8-isoprostane levels, a marker of oxidative stress (measured at 2 months after the surgery), in the triple NOSs^{-/-} mice (Fig. 6F).

3.7. Combined treatment with an angiotensin II type 1 (AT₁) receptor blocker, irbesartan, and an antioxidant calcium channel antagonist, amlodipine, markedly prevented coronary arteriosclerotic lesion formation and the occurrence of myocardial infarction and improved the prognosis of 2/3NX triple NOSs^{-/-} mice

Finally, in order to examine the involvement of renin–angiotensin system activation and oxidative stress in the pathogenesis of acute myocardial infarction in the 2/3NX triple NOSs^{-/-} mice, and also in order to validate the experimental usefulness of this acute myocardial infarction model, we investigated the effects on the cardiovascular abnormalities in this model of treatment with a selective and potent AT₁ receptor blocker, irbesartan; an antioxidant dihydropyridine calcium channel antagonist, amlodipine; a combination of both; or an

anti-hypertensive agent, hydralazine. We used the clinical therapeutic dosage of irbesartan and amlodipine. Single treatment with irbesartan or amlodipine markedly reduced the plasma angiotensin II levels, the cardiac ACE protein levels, and the urinary 8-isoprostane levels in the 2/3NX triple NOSs^{-/-} mice, while the combined treatment with irbesartan and amlodipine more potently decreased those values (Figs. 7A–C and Online Supplementary Fig. 3), although the data of the cardiac ACE protein levels again did not reach a statistically significant level owing to dispersion of the data (Fig. 7B and Online Supplementary Fig. 3). Mono-treatment with irbesartan or amlodipine significantly improved the survival rate in the 2/3NX triple NOSs^{-/-} mice, while the irbesartan/amlodipine co-treatment more powerfully ameliorated it. More importantly, these significant effects were noted within the short time of 4 months after the drug treatment, indicating the usefulness of this model for pharmacological studies (Fig. 7D). The sole treatment with irbesartan or amlodipine inhibited the incidence of myocardial infarction (the percentage of death due to myocardial infarction in the total causes of death) and coronary arteriosclerotic lesion formation (neointimal formation, medial thickening, and perivascular fibrosis) in the 2/3NX triple NOSs^{-/-} mice, while the simultaneous treatment with irbesartan and amlodipine more intensely prevented both the incidence of myocardial infarction (Fig. 7E) and coronary lesion formation (Figs. 7F–H). On the other hand, although the treatment with hydralazine significantly lowered systolic blood pressure in the 2/3NX triple NOSs^{-/-} mice to the same extent as the treatment with irbesartan plus amlodipine (Fig. 8A), it did not significantly affect the plasma angiotensin II levels, the cardiac ACE protein levels, the urinary 8-isoprostane levels, the survival rate, the incidence of myocardial infarction, or coronary lesion formation (Figs. 7A–H).

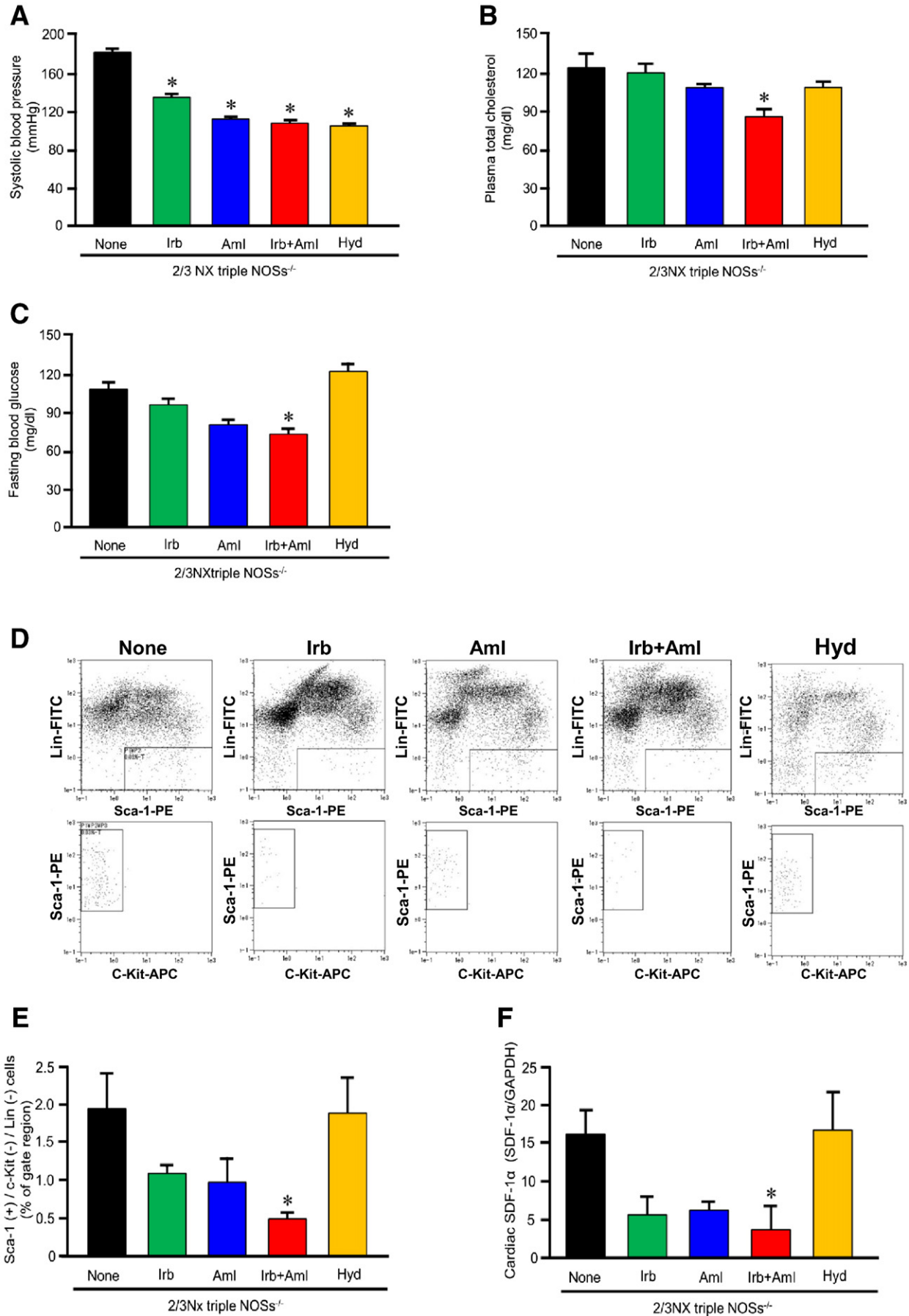
The treatments with irbesartan, amlodipine, and their combination significantly diminished the plasma creatinine levels and the urinary protein levels in the 2/3NX triple NOSs^{-/-} mice (Figs. 7I, J). The treatment with hydralazine also significantly attenuated the urinary protein levels, whereas it had no effect on the plasma creatinine levels (Figs. 7I, J). These results suggest that the decrease in the plasma creatinine levels might have been related to the renal protective actions of the pharmacological agents, while the reduction in the urinary protein levels might have been associated with the lowering of renal intraglomerular pressure induced by these anti-hypertensives.

The plasma total cholesterol levels and the fasting blood glucose levels in the 2/3NX triple NOSs^{-/-} mice tended to be lessened by the treatment with irbesartan or amlodipine, while statistically significant effects were noted only by the combined irbesartan/amlodipine treatment (Figs. 8B, C). Similarly, while the number of circulating Sca-1⁺/c-Kit⁻/Lin⁻ cells and the cardiac SDF-1 α protein levels in the 2/3NX triple NOSs^{-/-} mice tended to be suppressed by the irbesartan or amlodipine treatment, statistically significant effects were recognized exclusively by the simultaneous treatment with the two agents (Figs. 8D–F and Online Supplementary Fig. 4).

4. Discussion

The major novel findings of the present study are as follows: (i) 2/3NX caused sudden cardiac death due to acute myocardial infarction in male triple NOSs^{-/-} mice as early as 4 months after the surgery. (ii) The 2/3NX triple NOSs^{-/-} mice exhibited electrocardiographic ST-segment elevation, reduced heart rate variability, echocardiographic regional wall motion abnormality, and accelerated coronary

Fig. 7. Effects of treatment with an angiotensin II type 1 (AT₁) receptor blocker, irbesartan; an antioxidant calcium channel antagonist, amlodipine; a combination of irbesartan and amlodipine; or an anti-hypertensive agent, hydralazine, on renin–angiotensin system activation, oxidative stress, survival rate, incidence of myocardial infarction, coronary arteriosclerotic lesion formation, and renal function in the 2/3NX triple NOSs^{-/-} mice. Irb, irbesartan (50 mg/kg/day in chow); Aml, amlodipine (3.2 mg/kg/day in drinking water); Hyd, hydralazine (250 mg/mL in drinking water). The effects of the drugs on coronary lesion formation were assessed in the 2/3NX triple NOSs^{-/-} mice at 2 months after the surgery. (A) Plasma angiotensin II levels ($n = 10$). (B) Cardiac ACE protein expression levels ($n = 7$). (C) Urinary 8-isoprostane levels ($n = 8$). (D) Survival rate ($n = 20$ –49). (E) Percentage of death due to myocardial infarction in the total causes of death ($n = 6$ –49). (F) Neointimal formation (the ratio of intima area to media area) ($n = 6$ –16). (G) Medial thickening (the ratio of media area to total vascular area) ($n = 6$ –16). (H) Perivascular fibrosis (the ratio of perivascular area to total vascular area) ($n = 6$ –16). (I) Serum creatinine levels ($n = 10$). (J) Urinary protein levels ($n = 10$). * $P < 0.05$ vs. none (untreated control).



arteriosclerotic lesion formation. (iii) Cardiovascular risk factors (hypertension, hypercholesterolemia, and hyperglycemia), an increased number of circulating bone marrow-derived VSMC progenitor cells, and cardiac up-regulation of SDF-1 α were noted in the 2/3NX triple NOSs^{-/-} mice and were associated with significant increases in plasma angiotensin II levels and urinary 8-isoprostane levels. (iv) Simultaneous treatment with a clinical dosage of an angiotensin II type 1 receptor blocker, irbesartan, and an antioxidant calcium channel antagonist, amlodipine, markedly prevented coronary arteriosclerotic lesion formation and the incidence of myocardial infarction and improved the prognosis of those mice, along with ameliorating all those pro-arteriosclerotic parameters. Here we report the establishment of a new experimentally useful model of acute myocardial infarction.

4.1. Animal models that develops acute myocardial infarction

Five animal models that emerge acute myocardial infarction have thus far been reported. The first reported acute myocardial infarction model is a rat treated with a non-selective NOS inhibitor, such as N^ω-nitro-L-arginine methyl ester (L-NAME) or N^ω-nitro-L-arginine (L-NNA), chronically [20–23]. However, we clarified that arteriosclerotic vascular lesion formation caused by long-term treatment with L-NAME or L-NNA is not mediated by simple inhibition of NOSs activities [24]. While L-NAME- or L-NNA-treated rat shows multiple small infarcts without sudden death, those findings are quite different from human pathologies. The L-NAME- or L-NNA-treated rat has not been used at all as an acute myocardial infarction model. The second generated acute myocardial infarction model is the mouse with homozygous null mutations in the genes for both the high-density lipoprotein (HDL) receptor SR-B1 and apolipoprotein (apo) E [25]. The SR-B1^{-/-}/apoE^{-/-} mouse dies of acute myocardial infarction before 2 months of age (in childhood) even when fed a standard chow diet [25]. This short-term occurrence of acute myocardial infarction would be useful for experiments. However, the clinical course in human patients with acute myocardial infarction, which usually occurs in adulthood, is different from the natural course in the SR-B1^{-/-}/apoE^{-/-} mouse. The third produced model is the myocardial infarction-prone Watanabe heritable hyperlipidemic (WHHLMI) rabbit. The WHHLMI rabbit is not useful for experiments either because it takes a very long time (1 to 3 years) to develop acute myocardial infarction. The fourth created model is the SR-B1^{-/-}/hypomorphic apo ER61 (apoER^{h/h}) mouse, which shows high-fat diet-induced acute myocardial infarction [26]. Although the SR-B1^{-/-}/apoER^{h/h} mouse may be a good model, it has not been used at all in experiments in which the effects of drugs or therapies are examined since its generation was published 9 years ago, and only one article with this mouse has been published after the generation [27]. We reported a fifth model, the triple NOSs^{-/-} mouse, that spontaneously develops acute myocardial infarction. Unfortunately, however, it takes a very long time (approximately 1 year) for acute myocardial infarction to occur in our mouse. In the present study, the majority of the 2/3NX triple NOSs^{-/-} mice exhibited sudden cardiac death due to acute myocardial infarction within as little as 4 months after the surgery, and the experimental usefulness of this model was validated by demonstrating the preventive effects of the combined treatment with irbesartan and amlodipine on the occurrence of acute myocardial infarction. Therefore, our 2/3NX triple NOSs^{-/-} mouse is a new experimentally useful model of acute myocardial infarction.

Severe coronary arteriosclerosis, including infiltration of inflammatory cells, neointimal formation, medial thickening, and perivascular fibrosis, as well as coronary thrombus formation, was noted in the 2/3NX triple NOSs^{-/-} mice. These findings closely resemble the human pathology seen in the infarct-related coronary arteries in patients with myocardial infarction. We previously indicated that endothelium-dependent relaxations to acetylcholine are completely lacking in the triple NOSs^{-/-} mice and that contractions to phenylephrine are markedly enhanced, suggesting the presence of vascular dysfunction in the triple NOSs^{-/-} mice [11]. Thus, it is likely that acute myocardial infarction in the 2/3NX triple NOSs^{-/-} mice resulted from coronary arteriosclerosis, coronary thrombosis, and coronary vasospasm.

Heart rate variability is considered a noninvasive marker to evaluate autonomic nervous system function. It has been reported that low heart rate variability has prognostic value in patients with myocardial infarction and is associated with a higher risk of death in patients with coronary artery disease [28,29]. Consistent with the findings, significantly lower LF/HF ratio was noted in the 2/3NX triple NOSs^{-/-} mice.

4.2. Clinical implications

Several lines of evidence imply the clinical significance of the 2/3NX triple NOSs^{-/-} model. First, the natural course in which acute myocardial infarction occurs in the triple NOSs^{-/-} mice with partial nephrectomy closely resembles the clinical course in which patients with CKD develop acute myocardial infarction. Second, it has been suggested that the defective NOSs system is present in patients with CKD [30], as evidenced by the facts that in such patients urinary NOx excretion, a marker of systemic NO production derived from all three types of NOSs, are reduced [31], that whole body NO production (assessed by giving an intravenous infusion of [¹⁵N₂]-arginine and measuring isotopic plasma enrichment of [¹⁵N]-citrulline) is decreased [32], and that plasma levels of asymmetric dimethylarginine (ADMA), an endogenous NOS inhibitor, are elevated [33]. Finally, it has been reported that the defective NOSs system also exists in patients with coronary arteriosclerosis and myocardial infarction, as demonstrated by the findings that plasma and/or urinary NOx levels are reduced in such patients [34], that plasma ADMA concentrations are elevated in patients with arteriosclerosis and risk of myocardial infarction [35], and that the NOS gene polymorphisms are associated with arteriosclerosis, risk of myocardial infarction, and low plasma NOx levels in humans [36]. Thus, our acute myocardial infarction model may have clinical implications. However, since pathological conditions of the 2/3NX triple NOSs^{-/-} mice may be different from those of the patients with CKD, results obtained from our model must be interpreted with caution.

4.3. Mechanisms for acute myocardial infarction in the 2/3NX triple NOSs^{-/-} mice

Because significant increases in systolic blood pressure, plasma total cholesterol levels, and fasting blood glucose levels were noted in the 2/3NX triple NOSs^{-/-} mice, a clustering of cardiovascular risk factors seems to be involved in the pathogenesis of their acute myocardial infarction. In agreement with this evidence, it has been shown that patients with CKD have a high prevalence of those cardiovascular risk factors, and that those factors are associated with increased risks of acute myocardial infarction and sudden cardiac death [37].

It has recently been reported that bone marrow-derived mononuclear cells differentiate into VSMC progenitor cells, which circulate in

Fig. 8. Effects of treatment with an AT1 receptor blocker, irbesartan; a calcium channel antagonist, amlodipine; a combination of irbesartan and amlodipine; or an anti-hypertensive agent, hydralazine, on cardiovascular risk factors and SDF-1 α -induced recruitment of circulating bone marrow-derived VSMC progenitor cells in the 2/3NX triple NOSs^{-/-} mice. (A) Systolic blood pressure ($n = 10$ –12). (B) Plasma total cholesterol levels ($n = 10$ –12). (C) Fasting blood glucose levels ($n = 10$ –12). (D and E) The number of circulating Sca-1⁺/c-Kit⁻/Lin⁻ cells ($n = 7$). (F) Cardiac SDF-1 α protein levels ($n = 7$). * $P < 0.05$ vs. none (untreated control).

the blood, accumulate in vascular wall, and contribute to vascular lesion formation [38,39]. It has also been shown that the CXC chemokine SDF-1 α is a pivotal chemotactic factor of bone marrow-derived VSMC progenitor cells [40]. In the present study, the number of circulating Sca-1⁺/c-Kit⁻/Lin⁻ cells (interpreted as bone marrow-derived VSMC progenitor cells) [41] and the cardiac SDF-1 α protein levels were markedly increased in the 2/3NX triple NOSs^{-/-} mice. Thus, it is possible that SDF-1 α -induced recruitment of the circulating bone marrow-derived VSMC progenitor cells was also involved in the occurrence of acute myocardial infarction in the 2/3NX triple NOSs^{-/-} mice.

Renin-angiotensin system activation (as evidenced by increases in plasma angiotensin II levels and cardiac ACE expression levels) and oxidative stress (as indicated by elevation in urinary 8-isoprostane levels) were noted in the 2/3NX triple NOSs^{-/-} mice. Based on these findings, we used the selective and potent AT1 receptor blocker, irbesartan, and the antioxidant calcium channel antagonist, amlodipine, to further examine the involvement of renin-angiotensin system activation and oxidative stress in the pathogenesis of acute myocardial infarction. It has been indicated that amlodipine is a charged molecule, is highly lipophilic, and has a much higher affinity for lipid-laden cellular membranes than do other calcium channel antagonists, exerting a powerful antioxidant activity, independent of its calcium channel antagonistic action [42]. In the present study, the simultaneous treatment with irbesartan and amlodipine potently suppressed renin-angiotensin system activation and oxidative stress, and markedly prevented coronary arteriosclerotic lesion formation and the incidence of myocardial infarction, and improved the prognosis of the 2/3NX triple NOSs^{-/-} mice. Furthermore, the simultaneous irbesartan/amlodipine treatment significantly ameliorated the cardiovascular risk factors, the increased number of circulating Sca-1⁺/c-Kit⁻/Lin⁻ cells, and the enhanced cardiac SDF-1 α expression levels in those mice. Therefore, it is conceivable that renin-angiotensin system activation and oxidative stress are involved in the pathogenesis of acute myocardial infarction in the 2/3NX triple NOSs^{-/-} mice. Consistent with these results, it has been reported that renin-angiotensin system activation and oxidative stress are recognized in patients with CKD, and that both factors accelerate arteriosclerotic lesion formation [13].

The treatment with hydralazine exerted an anti-hypertensive action to the same extent as the combined treatment with irbesartan and amlodipine. However, the hydralazine treatment did not show any beneficial effects on the incidence of myocardial infarction, the prognosis, or the pro-arteriosclerotic parameters in the 2/3NX triple NOSs^{-/-} mice. Thus, it is suggested that the beneficial effects of the irbesartan/amlodipine treatment are not caused by changes of blood pressure.

4.4. Clinical perspectives

The mechanism(s) by which CKD is complicated by acute myocardial infarction is not fully understood. Our findings provide novel evidence that the NO/NOS system plays a pivotal role in the pathogenesis of this reno-cardiac connection. The AT1 receptor blockers and calcium channel antagonists are widely used to treat hypertension in patients with CKD, and the former are also employed to retard the progression of CKD. In the present study, the clinical dosage of irbesartan and amlodipine exhibited cardiovascular and renal protective actions in the 2/3NX triple NOSs^{-/-} mice. These results suggest the therapeutic importance of the AT1 receptor blockers and calcium channel antagonists in preventing complications of acute myocardial infarction in CKD as well as the progression of CKD.

4.5. Conclusions

We have succeeded in developing a novel experimentally useful model of acute myocardial infarction. Renin-angiotensin system activation, oxidative stress, cardiovascular risk factors, and SDF-1 α -induced

recruitment of circulating bone marrow-derived VSMC progenitor cells appear to be involved in the pathogenesis of acute myocardial infarction in the 2/3NX triple NOSs^{-/-} mice. This model may contribute to the elucidation of the pathogenesis of acute myocardial infarction, and to the research and development of novel therapeutic strategies for preventing this fatal cardiovascular disorder.

Sources of funding

This work was supported in part by a Grant-in-Aid for Scientific Research from the Japan Society for the Promotion of Science (23590305), Special Account Budgets for Education and Research granted by the Japan Ministry of Education, Grants from the Promotion Project of Medical Clustering of Okinawa prefecture and the University of the Ryukyus, and a Grant and Donation from the Sumitomo Dainippon Pharma Co, Japan. These funding sources had no involvement regarding the conduct of the research or preparation of the article.

Conflict of interest

We obtained irbesartan and amlodipine from the Sumitomo Dainippon Pharma Co, Japan, and received a research fund and donation from the company.

Appendix A. Supplementary data

Supplementary data to this article can be found online at <http://dx.doi.org/10.1016/j.jmcc.2014.09.021>.

References

- [1] White HD, Chew DP. Acute myocardial infarction. *Lancet* 2008;372:570–84.
- [2] Antman EM. ST-segment elevation myocardial infarction: pathology, pathophysiology, and clinical features. In: Libby P, Bonow RO, Mann D, Zipes DP, editors. *Braunwald's Heart Disease*. 9th ed. Philadelphia: Elsevier Saunders; 2012. p. 1087–110.
- [3] Antman EM, Loscalzo J. ST-segment elevation myocardial infarction. In: Longo DL, Fauci AS, Kasper DL, Hauser SL, Jameson JL, Loscalzo J, editors. *Harrison's Principles of Internal Medicine*. 18th ed. New York: Mc Graw Hill Medical; 2012. p. 2012–35.
- [4] Brecht DS, Snyder SH. Nitric oxide: a physiological messenger molecule. *Annu Rev Biochem* 1994;63:175–95.
- [5] Ignarro LJ. Biosynthesis and metabolism of endothelium-derived nitric oxide. *Annu Rev Pharmacol Toxicol* 1990;30:535–60.
- [6] Moncada S, Palmer RMJ, Higgs EA. Nitric oxide: physiology, pathophysiology, and pharmacology. *Pharmacol Rev* 1991;43:109–42.
- [7] Murad F. What are the molecular mechanisms for the antiproliferative effects of nitric oxide and cGMP in vascular smooth muscle? *Circulation* 1997;95:1101–3.
- [8] Shimokawa H. Primary endothelial dysfunction: atherosclerosis. *J Mol Cell Cardiol* 1999;31:23–37.
- [9] Tsutsui M, Shimokawa H, Otsuji Y, Yanagihara N. Pathophysiological relevance of NO signaling in the cardiovascular system: novel insight from mice lacking all NO synthases. *Pharmacol Ther* 2010;128:499–508.
- [10] Morishita T, Tsutsui M, Shimokawa H, Sabanai K, Tasaki H, Suda O, et al. Nephrogenic diabetes insipidus in mice lacking all nitric oxide synthase isoforms. *Proc Natl Acad Sci U S A* 2005;102:10616–21.
- [11] Nakata S, Tsutsui M, Shimokawa H, Suda O, Morishita T, Shibata K, et al. Spontaneous myocardial infarction in mice lacking all nitric oxide synthase isoforms. *Circulation* 2008;117:2211–23.
- [12] Coresh J, Selvin E, Stevens LA, Manzi J, Kusek JW, Eggers P, et al. Prevalence of chronic kidney disease in the United States. *JAMA* 2007;298:2038–47.
- [13] Lopez-Novoa JM, Martinez-Salgado C, Rodriguez-Pena AB, Lopez-Hernandez FJ. Common pathophysiological mechanisms of chronic kidney disease: therapeutic perspectives. *Pharmacol Ther* 2010;128:61–81.
- [14] Ninomiya T, Kiyohara Y, Kubo M, Tanizaki Y, Doi Y, Okubo K, et al. Chronic kidney disease and cardiovascular disease in a general Japanese population: the Hisayama Study. *Kidney Int* 2005;68:228–36.
- [15] Ninomiya T, Kiyohara Y, Tokuda Y, Doi Y, Arima H, Harada A, et al. Impact of kidney disease and blood pressure on the development of cardiovascular disease: an overview from the Japan Arteriosclerosis Longitudinal Study. *Circulation* 2008;118:2694–701.
- [16] Shoji T, Abe T, Matsuo H, Egusa G, Yamasaki Y, Kashihara N, et al. Chronic kidney disease, dyslipidemia, and atherosclerosis. *J Atheroscler Thromb* 2012;19:299–315.
- [17] Miyazaki-Anzai S, Levi M, Kratzer A, Ting TC, Lewis LB, Miyazaki M. Farnesoid X receptor activation prevents the development of vascular calcification in ApoE^{-/-} mice with chronic kidney disease. *Circ Res* 2010;106:1807–17.